Density dependence impacts our understanding of population resilience

Christina M. Hernández[a], Iain Stott[b], David Koons[c], and Roberto Salguero-Gómez[a]

[a]Department of Biology, South Parks Road, Oxford University, Oxford, UK
[b]School of Life and Environmental Sciences, University of Lincoln, Lincoln, UK
[c]Department of Fish, Wildlife, and Conservation Biology, Colorado State University, Fort Collins, Colorado, USA

Last compiled: September 27, 2024

Keywords: amplification, COMADRE, COMPADRE, life history strategy, matrix population model, reactivity, recovery time, transient dynamics

Acknowledgements We thank A. Hector and A. Compagnoni for comments on earlier versions of the manuscript. This work was supported by a NERC Pushing the Frontiers grant (NE/X013766/1) to RSG.

Conflict of Interest The authors declare none.

Author Contributions CMH and RSG conceived of the project. CMH and RSG performed analyses and prepared figures. All authors contributed to interpretation of results. CMH wrote the first draft, and all authors contributed to revising the text.

Data availability statement The data that support the findings of this study are openly available at www.compadre-db.org. Code will be archived in Zenodo and available at the time of publication in a peer-reviewed journal.

Abstract

Current metrics of demographic resilience (e.g., resistance, recovery) summarize the potential responses of populations to the frequent, varied disturbances that ecological systems experience. Much of the application of these metrics has focused on the potential response of time-invariant, density-independent structured population models to hypothetical disturbances. Here, we examine such resilience measures in a flexible structured model with five vital rate parameters. Making one vital rate density-dependent at a time, we show that density dependence has profound and complex impacts on our understanding of resilience. Depending on which vital rate was subject to density effects, existing measures of demographic resilience (compensation, resistance, and recovery time) either increased or decreased with population density. Moreover, the density-independent model underpredicted the recovery time of the corresponding density-dependent model, with a greater offset for species with longer generation times and higher iteroparity. Our findings demonstrate the importance of underlying non-linear processes when examining demographic resilience.

1 Introduction

Ecological systems are exposed to a variety of disturbances. In the broadest sense, a disturbance is any a/biotic impact that causes a temporary change in the underlying biological processes of a system, potentially pushing it away from its equilibrium. Examples of disturbances include a hurricane knocking down adult trees in a stand (Horvitz et al., 1995), pollutants decreasing fertility (Levin et al., 1996), or the introduction of an invader that leads to the decline of endemic species (Doody et al., 2009). As a result of frequent disturbances in natural systems (Turner, 2010), ecological systems may spend little time at equilibrium (Coulson, 2021; Hastings, 2010; Hastings et al., 2018). Consequently, a major focus of ecology is to understand how ecological systems respond to these myriad disturbances (e.g., Horvitz et al., 1995; McLauchlan et al., 2020; Paniw et al., 2017). As human-induced impacts on biodiversity continue (Butchart et al., 2010; Jaureguiberry et al., 2022) and the frequency of disturbances increases (Turner, 2010), there is an urgent need to identify which species are most likely to persist (Hare et al., 2016; Hernández-Yáñez et al., 2022; Urban, 2015). The study of 'resilience' holds promise for addressing this urgent need (Capdevila et al., 2020; Ingrisch and Bahn, 2018; Scheffer et al., 2015). At its core, resilience is related to concepts of stability: when perturbed, does the system return to its previous (equilibrium) state –and how quickly does it return– or do the dynamics change dramatically in such a way that the system is attracted to a new equilibrium (Hastings et al., 2018)?

In natural populations, the demographic resilience framework (Capdevila et al., 2020; Stott et al., 2011) describes how populations are expected to respond to perturbations to population structure. Population structure is the relative distribution of individuals in a population across different size, stage, or age classes. Perturbations to population structure might arise from, for example, fires (Sah et al., 2010), hurricanes (Horvitz et al., 1995),

or changes in hunting pressure (Coulson et al., 2004). This framework of demographic resilience (Capdevila et al., 2020; Stott et al., 2011) is based on matrix population models, where the fates and reproductive contributions of individuals that are classified by their age, size, and/or developmental stage are followed in discrete time (Caswell, 2001). In these models, the long-term deterministic behaviour of the population is growth at the rate $r = \log \lambda$, where λ is the leading eigenvalue of the population projection matrix. If λ is greater than 1, the population is predicted to grow in the long term, and if λ is less than 1, to decline. When the population follows this deterministic behaviour, the population maintains a stable distribution across classes: the relative size of each (st)age class is constant, while the total population size grows or declines. When the relative size of the (st)age classes changes, the short-term growth rate can vary dramatically from λ (Stott et al., 2011). Natural populations are generally near, but not at, their stable distributions (Williams et al., 2011), leading to mismatches between the expected and realized population growth rate over the short term. An important assumption in this demographic resilience framework is that the vital rates (e.g., survival, maturation, reproduction) that define the matrix population model are density-independent (Stott et al., 2011).

Vital rates are commonly affected by population density, with important implications for population and community dynamics. At the population level, negative density dependence can lead the population size to be stable, to cycle, or to follow chaotic dynamics; the outcome typically depends on the life history of the species (Neubert and Caswell, 2000). In Soay sheep (*Ovis aries*), interactions between climate and population density cause population size to cycle between increases and crashes (Coulson et al., 2001). When reproductive output is subject to negative density dependence, adult survival is more important to population dynamics and reproduction less important as population density increases (Layton-Matthews et al., 2019). At low population densities, low encounter rates

between individuals can significantly inhibit reproduction, driving small populations to extinction ("Allee effects" Courchamp et al. 1999). Meanwhile, at the community level, density-dependent regulation is crucial to our understanding of species diversity. Theory predicts that coexisting species should exhibit stronger intra-specific competition (i.e., within-population negative density dependence) than inter-specific competition (Chesson, 2000). This theoretical expectation is strongly supported by empirical evidence from plant communities, which overwhelmingly exhibit stronger intra- than inter-specific competition (Adler et al., 2018; Metz et al., 2010; Wills et al., 1997).

Matrix population models are generally evaluated at a particular density, rather than being constructed as explicitly density-dependent models (Crone et al., 2011). Even when density has been manipulated as part of the experimental design, these models are often constructed as 'high-density' and 'low-density' populations (Meekins and McCarthy, 2002; Oli et al., 2001). As a result, the vast majority of models archived in the COMADRE and COMPADRE databases (Salguero-Gómez et al., 2015; Salguero-Gómez et al., 2016a), which are among the largest repositories of published population models, do not explicitly include density effects. Since there is currently limited access to density-dependent matrix population models, past work on demographic resilience (Capdevila et al., 2022; Stott et al., 2011; Stott et al., 2012) has not taken density effects into account. This aspect is especially important since demographic resilience usually examines population change relative to disturbances in population structure and/or size. Currently, the implicit assumption is that a population's resilience is the same given a certain structure, regardless of overall population size. Under density dependence, this assumption is likely not to hold. Even given the same population structure and size, resilience could be different if density dependence operates differently through time in terms of life cycle stages and vital rates affected.

Here, we explore the implications of density-dependent vital rates on the study of demographic resilience. We take a virtual species approach by simulating density-dependent effects on the vital rates of a two-stage matrix population model. By varying the combination of vital rate values, we explore a wide range of possible life history strategies. With these models, we ask the following questions: (i) How would the unobserved effects of density change our interpretation of population resilience?, (ii) How do the effects of density on resilience depend on life history strategy? Finally, we investigate the difference in transient behaviour of the density-independent and density-dependent models to (iii) assess whether the density-independent models currently in use could predict qualitative behaviour of the density-dependent models. We conclude by suggesting that the discipline is insufficiently equipped to study demographic resilience in non-linear systems, and offer suggestions to expand our toolbox to examine populations in their natural settings.

2 Methods

To examine the role of density dependence on demographic resilience across a wide variety of life history strategies, we defined a two-stage population model following Neubert and Caswell (2000). The two stages of this model are non-reproductive and reproductive individuals, with new offspring being placed into the non-reproductive class. An important addition to the Neubert-Caswell model here is the potential for individuals to retrogress (i.e., move 'backwards' in their development) from the reproductive class to the non-reproductive class. Including retrogression is important for accurately representing the life cycles of many plants (Salguero-Gómez and Casper, 2010) and some animals (Cant et al., 2023; Wikelski and Thom, 2000) that have the ability to drastically decrease in size. For simplicity of language from this point on, we refer to the non-reproductive class as "juveniles" and the reproductive class as "adults." Since some life cycles are best under-

stood in terms of size, here we note that our framework also applies to size-based models, in which case readers might want to think of the classes as "small" and "large" individuals. The transition probabilities that link them would then be growth (instead of progression) and shrinkage (instead of retrogression).

$$\begin{bmatrix} n_j(t+1) \\ n_a(t+1) \end{bmatrix} = \begin{bmatrix} \sigma_j * (1-\gamma) & \phi + \sigma_a \rho \\ \sigma_j * \gamma & \sigma_a * (1-\rho) \end{bmatrix} * \begin{bmatrix} n_j(t) \\ n_a(t) \end{bmatrix} \tag{1}$$

The resulting model has five vital rates: juvenile survival probability (σ_j), juvenile progression probability (γ), adult survival probability (σ_a), adult retrogression probability (ρ) and adult per-capita reproductive output (ϕ). The population is projected forward in time by multiplying the population vector, composed of the current number of juveniles (n_j) and adults (n_a), by the projection matrix.

2.1 Density dependence in demographic parameters

To explore the effects of density on population resilience, we made each vital rate density dependent, such that individual performance decreases with increasing density (Bonenfant et al., 2009; Layton-Matthews et al., 2019; Shepherd and Cushing, 1980; Takada and Nakashizuka, 1996). For survival, progression, and reproductive output, we used an exponential form of negative density dependence (Eq. 2). We chose this form because Neubert and Caswell (2000) found that their matrix population models had a stable equilibrium (at certain vital rate combinations/ranges) for density dependence on any of the vital rates. The general form is

$$\alpha(N) = \alpha_{max} e^{-N}, \tag{2}$$

where α_{max} is the maximum value that a given vital rate can take, and $\alpha(N)$ is that vital rate's value at a given value of population density ($N = n_a + n_j$).

The only vital rate that did not follow this functional form in our model framework was retrogression (ρ). In plant systems, the optimal size decreases when resource availability or habitat suitability decreases (Csergő et al., 2017; Salguero-Gómez and Casper, 2011); the same occurs in some animals (Cant et al., 2023; Wikelski and Thom, 2000). Since a higher density implies lower per-capita resource availability, we would expect the mean size of individuals to decrease with increasing density. Therefore, when retrogression is density-dependent, we would expect retrogression probability to increase with higher population density. Rather than the exponential form in Equation 2, here we used a saturating functional form, where retrogression probability is 0 at very low densities ($N \approx 0$) and increases up to a selected maximum value (asymptotically):

$$\rho(N) = \rho_{max} \ln(N + 1) \tag{3}$$

To ensure that $\rho(1)$ would have a pre-determined value, we set ρ_{max} to $\frac{\rho(1)}{\ln 2}$. This value is the result of re-arranging Equation 2 to solve for ρ_{max}.

To compare the response to population density across a wide range of life history strategies, we re-scaled our models. The population densities of, for example, elephants and mice in a given unit of habitat area are on different orders of magnitude (Santini et al., 2018). Rather than being concerned with the absolute population densities, we examined demographic resilience when populations were 'far from carrying capacity' vs. 'near carrying capacity.' So, we scaled our models to a carrying capacity of 1, enabling us to examine the resilience of all life history strategies across the same range of population density values, from $N = 0$ to $N = 1$.

We carried out our scaling as follows. For each density-dependent vital rate 'case', we selected all parameters except for reproductive output (ϕ, or ϕ_{max} in the case of density-dependent reproductive output). Then, we solved for the value of reproductive output that

would cause the population to be at a stable equilibrium point at $N = 1$. The equations for reproductive output as a function of the other vital rates, for each density-dependent case, are given in Appendix Section S1. This scaling caused ϕ_{max} to be rather high for life history strategies with low survival. Indeed, to successfully invade, a species with low survival would have to produce a high number of propagules (Stearns, 1977). As σ_j, σ_a, and γ increased, the required ϕ_{max} decreased (Figure S1). This relationship also caused the population growth rate (λ) at low density to vary across life history strategies, with higher λ in shorter-lived life history strategies (Figure S2). Meanwhile, regardless of life history strategy, our scaling for a carrying capacity of 1 means that λ always equals 1 at a density of 1 (Figure S2).

2.2 Selecting virtual species

When all five vital rates can vary due to density dependence, the possible population models represent a large five-dimensional space. This would make it difficult to visualize how resilience and its response to density vary across life history strategies. To overcome this challenge, we selected a subset of 16 vital rate combinations that represent the 'space' of life history strategies as archived in the COMADRE (Salguero-Gómez et al., 2016a) and COMPADRE (Salguero-Gómez et al., 2015) databases. In their versions 4.23.3.1 and 6.23.5.0, these databases comprise 3,448 and 8,994 matrix population models for animals and plants, respectively. The majority of these models (>95%) have been digitized from the published literature. Here, we give a brief overview of how we used these databases to select our virtual species models. For the full details, see Appendix Section S2.

We first defined a subset of high-quality models from the COMADRE and COMPADRE databases that represent wild populations under control ("unmanipulated") conditions. Next, we collapsed each of those selected models to the same 2×2 matrix form given in

Equation 1 following (Salguero-Gómez and Plotkin, 2010), using the `mpm_collapse` function in the `Rage` package (Jones et al., 2022). Finally, we performed a principal component analysis (PCA) on the collapsed empirical matrix population models to project the five vital rates into a reduced dimensional space (Figure S3). We retained the first two principal component (PC) axes because together they captured 70% of the variation among models from COMADRE and COMPADRE (PC1: 43.83%; PC2: 26.25%). PC1 was primarily explained by variation in survival (σ_j, σ_a) and progression (γ), such that longer-lived and late-maturing species score positively on PC1, while short-lived and fast-maturing species score negatively. PC2 was primarily influenced by reproductive output (ϕ), such that species with high reproductive output score positively on PC2 (Supplemental Table S1). As such, we refer to virtual species that fall in the upper left quadrant (low scores on PC1 and high scores on PC2) as exhibiting fast life histories, and we refer to those that fall in the lower right quadrant (high scores on PC1 and low scores on PC2) as exhibiting slow life histories.

To define our virtual species, we inspected the distribution of empirical values of vital rates in our final set of 1,285 collapsed two-stage models. Based on these distributions, we selected a high and low value for juvenile survival (σ_j), juvenile progression (γ), and adult survival (σ_a) (Table S2). For retrogression (ρ), we set the low value as 0 (no retrogression at all), and we set our high value near the mean of empirical values in models from the databases where retrogression was greater than 0 (Table S2). We then projected our virtual species models across density-dependent scenarios onto the PC axes as defined by the empirical models. Our virtual species models cover the space of naturally observed populations reasonably well (Supplemental Figure S3). Based on our model scaling, for some virtual species and density-dependent vital rate scenarios, the virtual species plotted at much higher values of PC2 than seen in the empirical models (Supplemental Figure S4).

For plotting and analyses, we restricted the virtual species to combinations of vital rates and density-dependent scenarios that had a score on PC2 of ≤ 5.1 for population densities between 0 and 1.

2.3 Density-independent resilience metrics

We explored how population density, via effects on individual vital rates, would impact previously-studied metrics of demographic resilience (Capdevila et al., 2020; Stott et al., 2011). These previously-studied metrics are density-independent, but we can calculate them for a population projection matrix built at a particular density. In essence, we analyzed how our understanding of resilience would change if demographers had measured vital rates when the population was at low density vs. high density. To do so, we calculated *compensation*, *resistance*, and *recovery time* for the (density-independent) population projection matrix built from vital rates at various values of density between $N = 0$ and $N = 1$ (Figure 1A).

Compensation is the propensity for a population to 'boom' after a disturbance. Compensation is calculated as the largest possible population size, relative to a population growing at a rate λ, in the first time step after a disturbance (Capdevila et al., 2022). In general, this maximum one-time-step population growth rate would occur when the entire population is concentrated in the most fecund stage class. In our two-stage model, this situation corresponds to a scenario where only adults remain after a disturbance.

Resistance is the ability of a population to prevent further losses after a disturbance. Resistance is calculated as the smallest possible relative population size in the first time step after a disturbance (Stott et al., 2011). In general, this minimum one-time-step population growth rate would be achieved if the entire population were concentrated in the most vulnerable and least fecund stage class (e.g., juveniles in our two-stage model). Populations

can vary greatly in their degree of resistance from those whose abundance changes little following a disturbance even when individuals are concentrated in the most vulnerable and least fecund class (high resistance, metric close to 1) to those whose abundance crashes (low resistance, metric close to 0).

Recovery time is here defined as the number of time steps until all possible stage-biased trajectories converged back to asymptotic dynamics. A stage-biased trajectory has an initial condition (i.e., following a disturbance) where all remaining individuals are in a single stage class. For each possible stage-biased initial condition, we iterated the population model until the one-step-ahead population growth converges to λ using the `convt()` function in the `popdemo` package (Stott et al., 2012). We then measured recovery time as the maximum time across the possible initial conditions. In our model, there are two possible stage-biased initial conditions: only adults, and only juveniles. Note that this definition of recovery time is a change from recent publications on demographic resilience which used a definition of recovery time closely based on the damping ratio (e.g., Capdevila et al., 2020; Capdevila et al., 2022). Past analyses have indicated that the damping ratio is a poor measure of time to convergence (Stott et al., 2011). All density-independent resilience metrics were calculated using the `popdemo` package in R (Stott et al., 2012).

We analyzed the relationships between vital rates and resilience metrics in our virtual species using linear regression models in R (R Core Team, 2023). For each resilience metric, we fit two separate regression models. First, we fit a linear regression with strictly additive terms for all five vital rates. Second, we fit a linear regression for the first two principal component axes including additive terms and their interaction. We used these models to interpret the importance of different vital rates and the PC axes in driving the values of compensation, resistance, and recovery time by focusing on the effect sizes (i.e., regression coefficients). However, we do not report p-values because statistical power is

artificial in virtual species approaches (White et al., 2014), such as the one presented here. In essence, any desired p-value could be achieved by modulating the sample size and the level of replication of each virtual species across multiple density values for multiple vital rate scenarios.

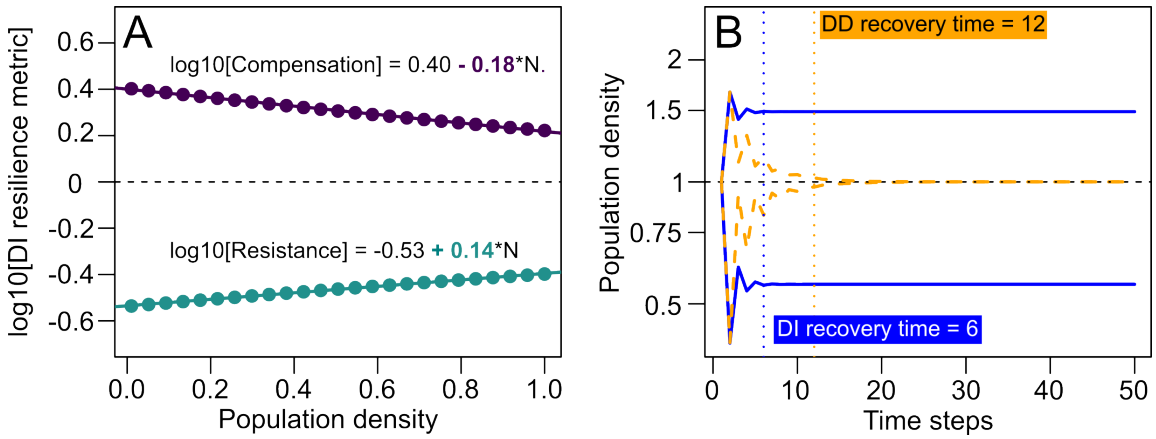

Figure 1: Examples for some key calculations regarding demographic responses to disturbances using transient dynamics. In both examples, reproduction decreases with increasing population density, and the vital rates are juvenile survival $\sigma_j = 0.4$, juvenile progression γ=0.9, adult survival $\sigma_a = 0.6$, and adult retrogression probability ρ=0. (A) At each value of population density (the plotted points), we calculated the density-independent resilience metrics (compensation in purple, resistance in green) from the density-independent matrix population model evaluated at the corresponding value of population density. We then fit a line to the $\log_{10}$-transformed resilience metrics, finding in this example that compensation decreased with population density (negative slope), while resistance increased with population density (positive slope). Note that we also calculated the slope of density-independent recovery time in the same way. (B) The recovery process of a density-independent and density-dependent model are distinct, even when they start from the same initial conditions. For this combination of vital rates, the density-independent model requires six time steps to recover back to asymptotic dynamics. Meanwhile, the density-dependent model requires 12 time steps to recover back to the carrying capacity.

We also explored how life history strategy interacted with density-dependent effects on resilience metrics. To do so, we calculated the slopes of log_{10}-transformed compensation, resistance, and recovery time with population density using the `lm` function in `R` v.4.3.2 (R Core Team, 2023) (Figure 1A). We calculated these slopes for each combination of juvenile survival, progression, adult survival, and retrogression across the full range of

possible values for those vital rates. To examine broad differences across density-dependent scenarios, we plotted the distributions of slopes for each resilience metric as histograms for each density-dependent scenario. To relate these slopes to life history strategy, we focused on how slopes changed across the full range of possible values of adult survival (σ_a) and progression (γ). For a subset of virtual species across the full range of adult survival and progression but with a single value of juvenile survival ($\sigma_j = 0.6$) and retrogression ($rho = 0.3$), we plotted the slopes as colour contours using the `levelplot` function from the `lattice` package (Sarkar, 2008). We chose these two vital rates because of their clear mathematical connection with generation time (Gaillard et al., 2005), which is itself an important proxy for life history speed (Healy et al., 2019; Paniw et al., 2018; Salguero-Gómez et al., 2016b). When progression rate is high and adult survival is low, species would exhibit precocious maturation and short mature life span, leading to a short generation time–we refer to this type of life history as 'fast.' Conversely, when progression rate is low and adult survival is high, species would have delayed maturation and long mature life span, leading to a long generation time–therefore this would be a 'slow' life history.

2.4 Analysis of transient envelopes

The addition of density-dependence to vital rates in the population models we explored here fundamentally changed the transient dynamics of those models. Not only did the density-independent metrics of resilience change with population density, but the process of recovery itself changed. This is because the density-dependent model will be attracted back to its equilibrium population size (a single point), while the density-independent model will be attracted to the asymptotic growth rate (a curve) (Figure 1B). Following Stott et al. (2011), we projected our virtual species forward in time from an all-juvenile or all-adult post-disturbance distribution, starting from a population density of 1. For

the first time step, the density-dependent and density-independent models are the same (Figure 1B). However, the entries of the density-dependent matrix model vary through time as density affects its target parameter: one of the five vital rates in our two-stage matrix population model (Eq. 1).

We examined whether the density-independent transient period is predictive of the density-dependent transient period. To that end, we calculated the recovery time in both models, and compared them. In the density-independent model, the recovery time is (as explained above) the elapsed time before both the upper and lower transient bounds return to following asymptotic dynamics (Stott et al., 2012). Because the transient bounds are calculated by iterating the standardised model ($\hat{\mathbf{A}} = \mathbf{A}/\lambda$; Stott et al. 2011), population size in the standardised model stops changing when the model converges (solid blue line in Fig. 1B). In the density-dependent model, the transient bounds will both eventually return to a population size of 1, the carrying capacity we pre-defined for our density-dependent models (dashed orange line in Fig. 1B). We defined the density-dependent recovery time as the time until the distance between the upper and lower bound was smaller than 0.1; this distance could be achieved when both bounds cross within 5% of the carrying capacity, or when one of the bounds has reached carrying capacity and the other is 0.1 population size units away. To compare these two values of recovery time, we defined the difference in recovery time ($\Delta RecoveryTime$) as the difference between the density-independent definition of recovery time (`convt()` from the `popdemo` package; Stott et al. 2011) and the density-dependent definition of recovery time (as defined here).

We also investigated how life history traits relate to the convergence time of the density-dependent model. We focused on generation time as a proxy for the position of the species along the fast-slow continuum (Gaillard et al., 2005), and the degree of parity as a measure of reproductive strategy (Salguero-Gómez et al., 2016b). For generation time, we calculated

the average age difference between parents and offspring (Bienvenu and Legendre, 2015). For degree of parity, we calculated Demetrius' entropy, which measures how spread out reproduction is across an individual's lifespan (Demetrius, 1977). Previous research has shown that both life history traits adequately capture a species' life history strategy (Healy et al., 2019; Paniw et al., 2018; Salguero-Gómez et al., 2016b). For both life history traits, we used the functions `gen_time` and `entropy_d`, respectively, from the `Rage` package (Jones et al., 2022).

We note that, in our comparisons of density-dependent and density-independent measures of convergence time, we present p-values for correlation coefficients and an ANOVA analysis. In this section, each combination of a virtual species and density dependence scenario occurs at most once, for a sample size of 54 models. We acknowledge that the p-values are a tenuous measure of significance (see White et al. 2014), but we argue that the p-values provide a useful benchmark for examining the patterns resultsing from our analyses.

3 Results

Density dependence affected our interpretation of demographic resilience. The strength and direction of the impact of density dependence on resilience metrics depended on both life history strategy and the specific vital rate target of density dependence. Because of our model scaling, faster life histories exhibited stronger density-dependent effects on their overall population growth rate (Figure 2A). Indeed, because we scaled the reproductive output (ϕ) so that all virtual species would have a carrying capacity of 1, fast life histories have high reproductive output and high values of population growth rate (λ) at low density, as evidenced by red colour (low λ) being associated with small points (low density), in the top-left area of Figure 2A (fast life history space). Equivalent patterns are not as

pronounced in the bottom right of the figure (slow life history space).

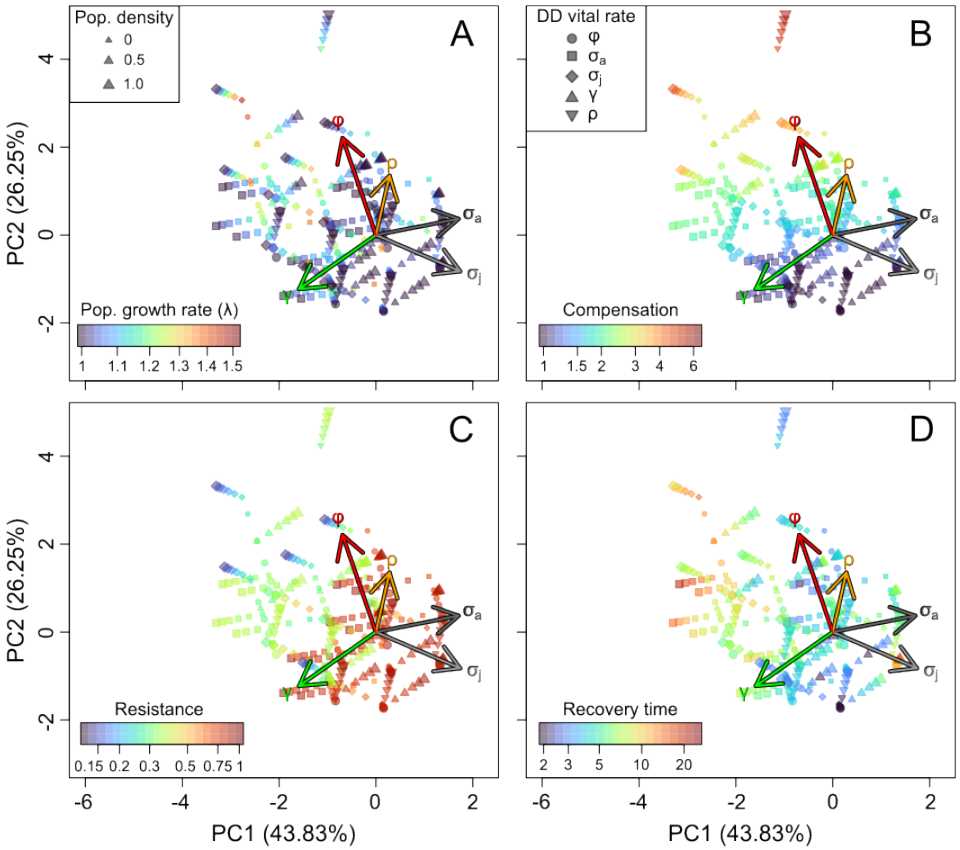

Figure 2: Resilience metrics in virtual species models change across life history strategies and density-dependent scenarios for (A) population growth rate, (B) compensation, (C) resistance, and (D) recovery time. The vital rates are: juvenile survival (σ_j), adult survival (σ_a), juvenile progression (γ), adult retrogression (ρ), and reproductive output (ϕ). The principal component (PC) axes were defined by the matrix population models parameterised with data from natural/wild populations under control conditions from 1,285 populations of animals and plants (see Figure S3). The virtual species have then been projected onto the PC axes. Life history speed generally increases with PC2 (increasing reproductive output), and decreases with PC1 (increasing survival), such that slow life histories are located towards the bottom-right of the PCA space and fast life histories are located towards the top-left. Each virtual species was modelled with density-dependence on each of the five vital rates (see top-right insert in panel B). For each density-dependent scenario, the virtual species model was calculated for six values of density between 0 and 1 (plot symbols sized according to population density).

In our virtual species models, compensation was most strongly influenced by repro-

ductive output (Figure 2B, Supplemental Table S3). Although most vital rates influenced compensation, the coefficients were both positive and negative (Supplemental Table S3). As a result, the effect of PC1 on compensation was much smaller than the effect of PC2 (Supplemental Table S3). As such, virtual species with higher reproductive output and faster life histories exhibited higher compensation (redder colours in the upper left of Figure 2B). Conversely, resistance was highest in species with slow life histories (redder colours to the lower right of Figure 2C). Resistance was most strongly influenced by juvenile survival, with limited influence from other vital rates (Supplemental Table S3). Recovery time decreased with adult survival and juvenile survival, but increased with retrogression (Supplemental Table S3). As a result, recovery time was longest in virtual species with low survival and high retrogression (redder colours to the far left in Figure 2D).

Compensation either increased or decreased with population density, depending on the vital rate that was affected by density dependence (Figure 3). Compensation always decreased at higher population density (negative slope) when reproductive output was density dependent, and always increased at higher population density (positive slope) when density-dependence acted via juvenile survival (Figure S5). When density dependence operated via adult survival, the response of compensation to density was rather weak (Figure 3), with the distribution of slope values centered on 0 (Figure S5). For progression and retrogression, compensation tended to increase with density (positive slopes; Figure 3), although the distribution crossed 0 (Figure S5). The response to density was clearly stronger when reproductive output or juvenile survival were density-dependent (absolute value of mean slope ≈ 0.2, Supplemental Figure histograms), in agreement with our results in Figure 2B that compensation was most closely related to reproductive output and juvenile survival.

In general, fast and slow life histories exhibited similar slopes of compensation across

densities (Figure 3). In other words, moving from a fast to a slow life history did not indicate a change in how strongly compensation would respond to density when reproductive output, progression, and juvenile survival were density dependent (see how the color contours in Figure 3 connect the upper left and lower right corners of the panels for ϕ, γ, and σ_j). However, when retrogression was density-dependent, then the strongest response of compensation to population density was in species with a slow life history (delayed progression and high adult survival).

Resistance tended to increase with population density in all scenarios except for density-

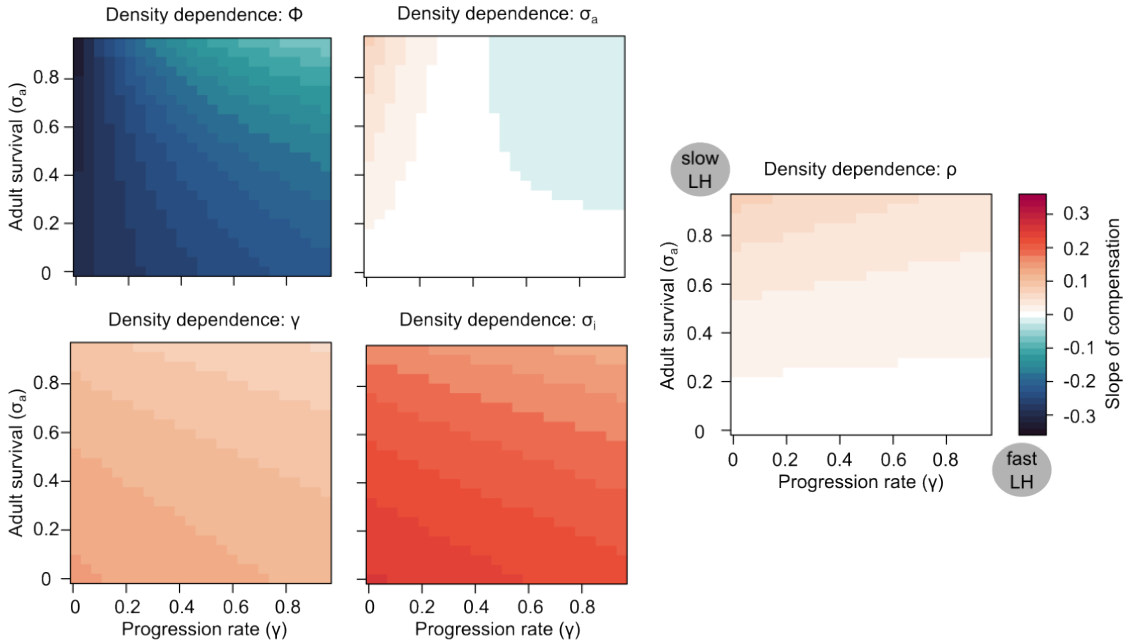

Figure 3: Strength of density effects on compensation varies with both life history strategy and density-dependence scenarios. The color contours indicate the slope of compensation as a function of population density. Redder colors indicate that compensation increased with increasing population density, while bluer colors indicate that compensation decreased with increasing population density. Slow life histories are in the upper left of each panel, and fast life histories are in the lower right. These slope surfaces are shown for models with intermediate juvenile survival $\sigma_j = 0.6$ and with retrogression rate $\rho = 0.3$ To see how slope changed across juvenile survival σ_j and adult retrogression ρ values within each scenario, see Figures S10-S9.

dependent juvenile survival (Figure 4 and S11). Like for compensation, the strongest response to population density was observed for the density-dependent reproductive output and juvenile survival cases. When reproductive output was density-dependent, resistance increased with population density most strongly in fast life histories, and the response was weaker in slow life histories. When juvenile survival was density-dependent, changes in slope were not related to life history speed; instead, the steepest slope emerged when individuals matured early and had high adult survival (Figure 4).

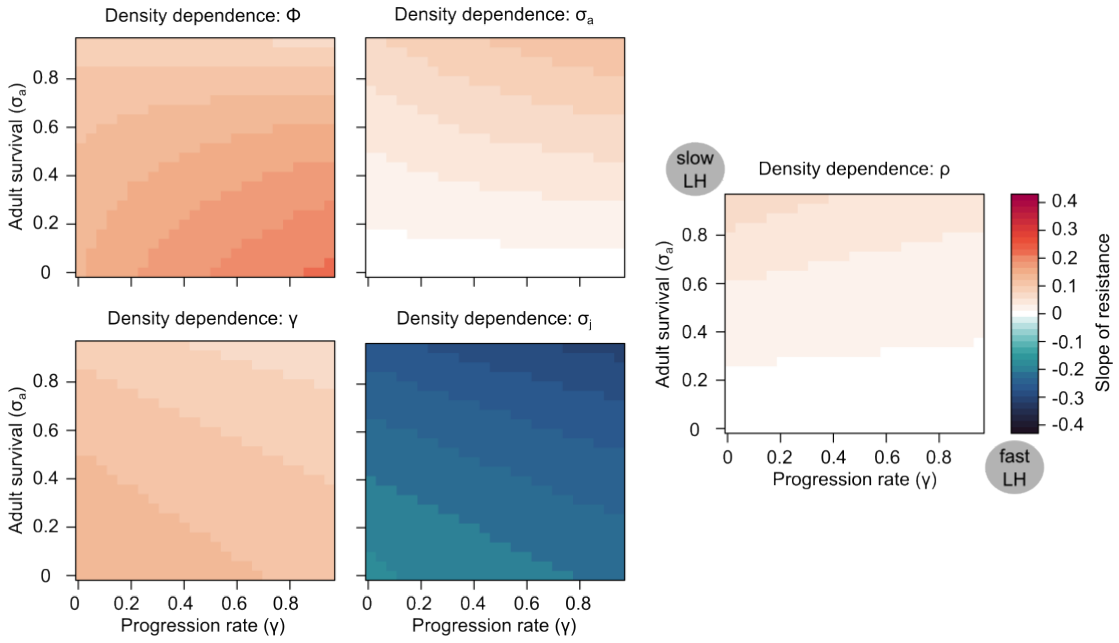

Figure 4: Strength of density effects on resistance varies with both life history speed and density-dependence scenarios. The color contours indicate the slope of resistance as a function of population density. Figure details are the same as in Figure 3. To see how slope changed across σ_j and ρ values within each scenario, see Figures S16-S15.

Responses of recovery time to changes in population density were highly variable (Figure 5). The steepest slopes of recovery time with density were seen when progression or reproductive output were density-dependent. When progression or reproductive output

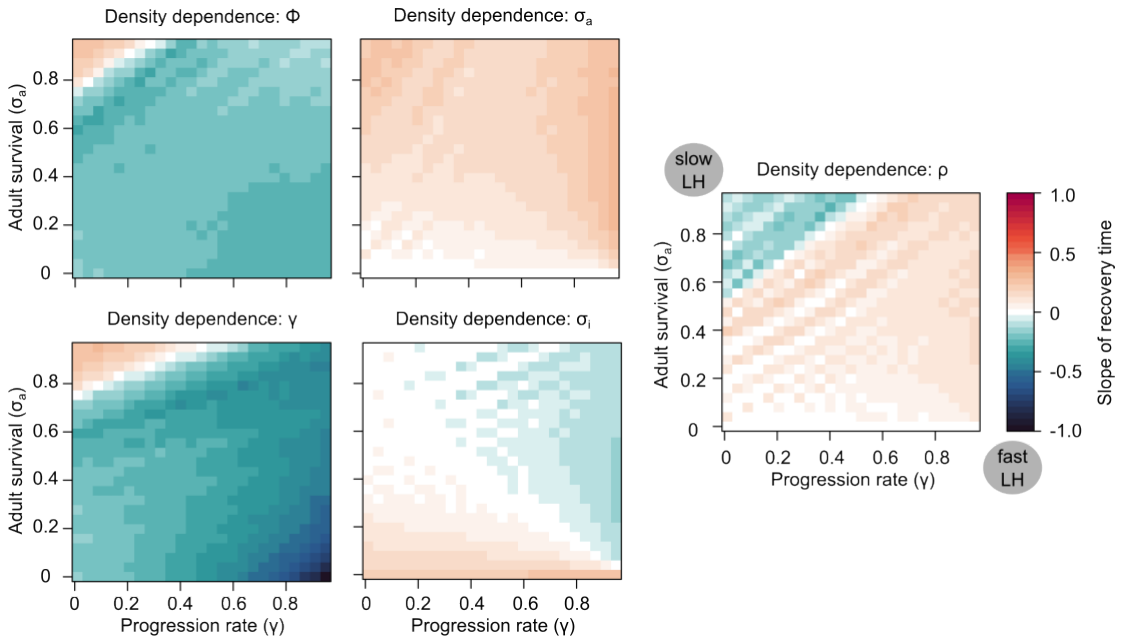

Figure 5: Strength of density effects on recovery time varies with both life history strategy and density-dependence scenarios. The color contours indicate the slope of recovery time as a function of population density. Figure details are the same as in Figure 3. To see how slope changed across juvenile survival σ_j and adult retrogression ρ values within each scenario, see Figures S22-S21.

were density-dependent, recovery time decreased at higher population densities for slow life histories, and recovery time increased at higher population densities for fast life histories (Figure 5). In the other vital rate cases, the response of recovery time to changes in density did not follow any consistent patterns.

Adding density dependence to our demographic models fundamentally changed the process of recovery, as shown in Figure 1B. Because we tuned our models such that the carrying capacity is at a population size/density of 1, we can compare the transient envelopes from the density-independent and density-dependent cases. We show one example in Figure 1B, but note that the shapes of the transient envelopes can vary dramatically across our virtual species and depending on which vital rate is density-dependent (Supplemental Figures

S23-S27).

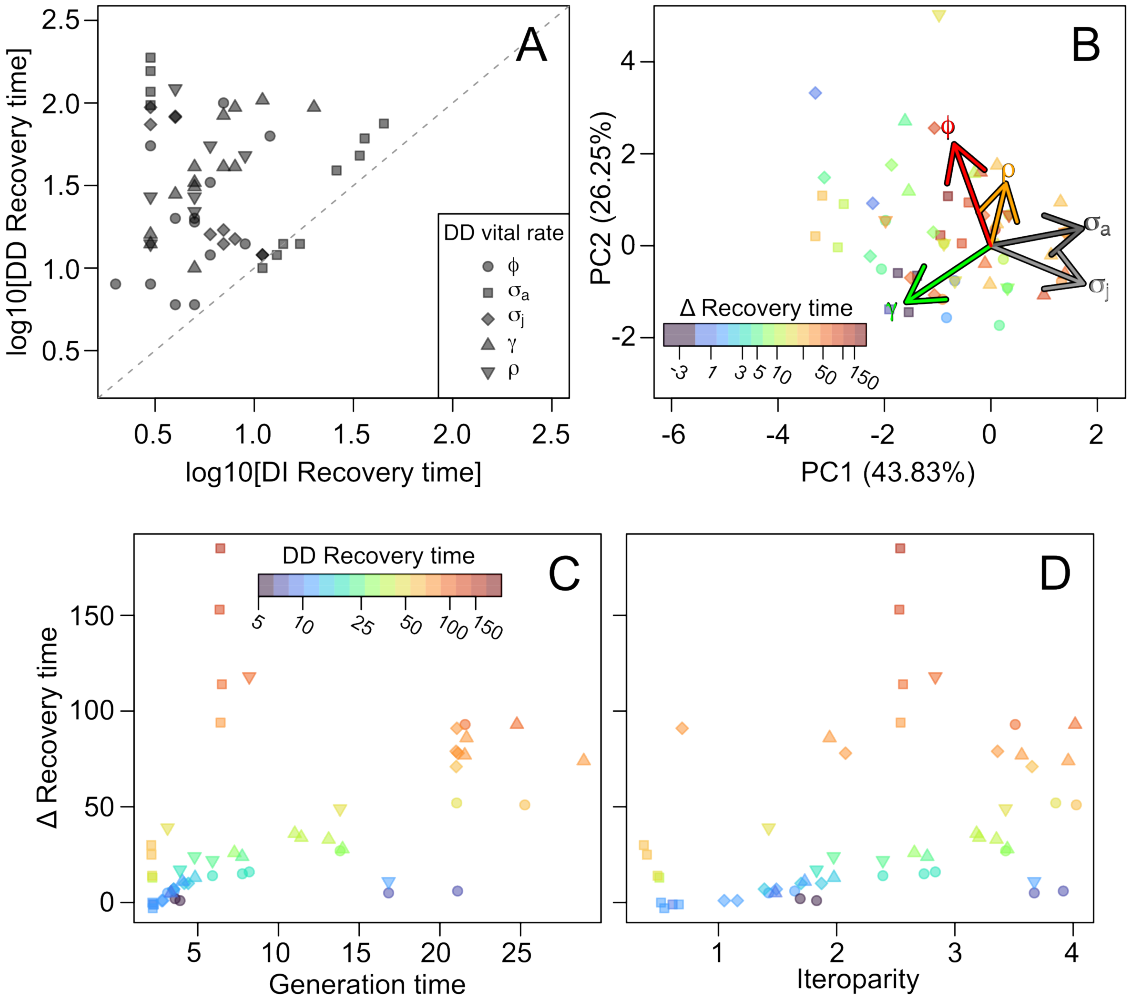

Figure 6: The density-independent (DI) model under-predicts recovery time compared with the density-dependent (DD) model. Panel A shows the relationship between density-independent recovery time and density-dependent recovery time for the virtual species models. Panel B shows the same virtual species on the PCA space as in Figure 2, colored according to $\Delta RecoveryTime$. Panels C and D show how $\Delta RecoveryTime$ relates to the generation time (C) and degree of iteroparity (D). The different shapes, across all panels, indicate the different density-dependent vital rate scenarios. The color scale shown in panel C applies to panel D as well.

The recovery time of the density-independent model nearly always under-predicted the

recovery time of the density-dependent model, without a significant relationship between the two recovery time measures ($r = 0.03, p = 0.80$; Figure 6A). There was no pattern to the offset between recovery time in the density-dependent and density-independent models ($\Delta RecoveryTime$) based on which vital rate was the target of density dependence (ANOVA $F_{4,49} = 0.787$, $p = 0.54$). In the vital rate PCA space, $\Delta RecoveryTime$ increased along PC1 ($\Delta RecoveryTime = \beta_1 * PC1 + \beta_2 * PC2$: $\beta_1 = 11.8$, p=0.01; $\beta_2 = 8.1$, p=0.12), indicating that species with greater survival and delayed progression should take longer to recover (Figure 6B). Moreover, we found a significant correlation of $\Delta RecoveryTime$ with both generation time ($r = 0.44, p < 0.001$) and iteroparity ($r = 0.37, p = 0.005$). In other words, as generation time increased or species became more iteroparous, the density-independent model was worse at predicting recovery time of the density-dependent model. If adult survival was density-dependent, then the density-independent model performed particularly poorly (Figure 6C and D).

4 Discussion

In the face of myriad disturbances that characterise the Anthropocene, the study of resilience promises to help ecologists and managers identify the species and ecosystems most likely to persist (Enquist et al., 2024). Resilience is closely related to concepts of stability (Hastings et al., 2018) and, in demographic models, long-term asymptotic system behavior (Capdevila et al., 2020; Stott et al., 2011). Although population density has important impacts on individual and population performance (e.g., Bonenfant et al., 2009; Layton-Matthews et al., 2019; Takada and Nakashizuka, 1996), density-dependence has been neglected in past studies of demographic resilience. Here, we show that density dependence has profound and complex impacts on our understanding of demographic resilience. Depending on which vital rate (e.g., survival, reproduction) is subject to density

effects, existing measures of demographic resilience (compensation, resistance, and recovery time sensu Capdevila et al. 2022; Stott et al. 2011) can either increase or decrease with population density. Importantly, the strength of density-dependence in our resilience metrics was often uncorrelated with life history speed: the apparent resilience of fast and slow life histories often responded the same way to density-dependence. We also found that the recovery time of a density-independent model did not predict the recovery time of the corresponding density-dependent model. In fact, the offset between the density-dependent and density-independent definitions of recovery time were correlated with life history: in species with longer generation time and greater iteroparity, the density-independent model is even worse at predicting recovery time of the underlying density-dependent dynamics.

Our results generally agree with past examinations linking metrics of demographic resilience and life history traits. For instance, using 162 populations of 69 animal species from COMADRE and 748 populations of 232 plant species from COMPADRE, all explicitly density-independent, Capdevila et al. (2024) showed that species with high reproductive output compensate more, resist less and tend to take longer to recover. Here, we found the effects of reproductive output on compensation, resistance, and recovery time to be in the same direction as previously reported, but the effect of reproductive output was only dominant over other vital rates in the relationship with demographic compensation. Generation time, a strong marker of life history speed (Gaillard et al., 2005), was found to influence the transient dynamics across 111 mammal species (Gamelon et al., 2014). Additionally, Capdevila et al. (2022) found that slow life histories take longer to recover following a disturbance. In agreement with this finding, here we report longer recovery times for slow life histories, as well as more severe under-estimation of recovery time in the density-independent compared with density-dependent model ($\Delta RecoveryTime$). These authors also found kingdom-specific responses for resistance: resistance increases with generation

time in animals but decreases in plants (Capdevila et al., 2024). These kingdom-specific responses may be linked via the more frequent ability of plants to shrink (Salguero-Gómez and Casper, 2010) than in animals (but see Wikelski and Thom 2000), an aspect that can be explicitly explored in future steps via our flexible structured population model. Regardless, the general agreement between both studies and ours, despite their lack of explicit consideration of density dependence, may be due to their strict data selection criteria, which might have implicitly incorporated self-regulation effects in the matrix models.

In some cases, we found counter-intuitive relationships between resilience and density. For example, when juvenile survival was density-dependent, compensation increased with population density. This counter-intuitive result arises from an indirect effect of density on compensation, via the direct effect of density on population growth rate (λ). Compensation is calculated as the maximum column sum of the standardized population matrix ($\hat{\mathbf{A}}$). Given that survival rates are bounded between 0 and 1, while fertility rates are often greater than 1 (Salguero-Gómez et al., 2015; Salguero-Gómez et al., 2016a), compensation is often determined by the fertility entries. Therefore, in our two-stage model, compensation is determined by the second column sum of $\hat{\mathbf{A}}$. So how does the density effect on juvenile survival, which appears only in the first column, impact compensation? The change in compensation arises because of the standardization ($\hat{\mathbf{A}} = \mathbf{A}/\lambda$). As juvenile survival decreases with density, λ decreases, and so the sum of the second column of $\hat{\mathbf{A}}$ actually increases. The same general principle applies for each of the vital rate scenarios where resistance increased with increasing density. This indirect effect of vital rates on resilience via a change in λ is both striking and easily interpreted in our two-stage model, but we may expect different results in larger, more complex life cycles and their resulting structured population models. Unlike the 2×2 model that we used here, most (93%) matrix population models archived in COMADRE and COMPADRE have more than two stages. In fact, 89%

of the models that we used for selecting our virtual species model were 3×3 or larger, and 53% of them were 5×5 or larger (Supplemental Figure S28).

Our findings have important implications for the study of invasive species. Amplification (here referred to as compensation), one of the three key components of demographic resilience (Capdevila et al., 2020), has recently been reported to be a strong predictor of invasiveness (Iles et al., 2016; Jelbert et al., 2019). However, neither of these two works dealt with models that explicitly incorporated density dependence - although we did find here that compensation and reproductive output are correlated in density-dependent models. Early in the invasion of a species, logically population size (and thus density) tends to be low, a feature that has attracted much attention via the so-called 'paradox of invasion' (Sax and Brown, 2000). However, the extent to which amplification remains a good predictor of performance of invasive populations as they become established, and how amplification may clarify the paradox of invasion, are promising next steps of research.

Our findings clearly highlight the need for more research aimed at understanding the role of density dependence in populations at risk of extinction. We found that the currently-available density-independent demographic models underestimate recovery time if the underlying vital rates are density-dependent. The underestimation of recovery time was most severe when species have long generation times and/or high iteroparity. Because animal species with long generation times are also more vulnerable to extinction under climate change (Pearson et al., 2014), understanding how these species respond to changes in population density may be most urgent. Interestingly, generation time does not appear to be a strong predictor of extinction risk in plants (Hernández-Yáñez et al., 2022; Salguero-Gómez, 2017), suggesting that different processes may be most important. In vertebrates, the vital rates with the strongest evidence of density dependence are age or size of maturity (e.g. progression in our model) and reproductive output (Bassar et al., 2010). Meanwhile,

we found that resilience was most impacted by density-dependent effects when either reproductive output or juvenile survival were the targets of density dependence. Taken together, this suggests that density effects on reproductive output may be the best place to start integrating density-dependence into demographic models.

The existing framework of demographic resilience is insufficient to examine the trajectory of a density-dependent model after a disturbance. Instead of analysing the demographic resilience of a fully-specified density-dependent matrix population model, we built a series of hypothetical density-independent models by calculating the vital rates that a population would have at each population density. We were constrained to this approach because the framework of demographic resilience relies on analysis of population size relative to the asymptotic population growth and requires that populations start from a population size/density that is standardised to 1 following a one-off (i.e., pulse) disturbance (Stott et al., 2011; Stott et al., 2012). These generalisations make less sense in a density-dependent scenario where the model has an asymptotic population growth rate (λ) of 1 (no net growth once the population reaches equilibrium). Instead, for density-dependent models, measuring relative to carrying capacity is more relevant and encompasses elements of both population size and asymptotic stability. Indeed, in our models we set carrying capacity, rather than initial population size, to equal 1. As a result, our density-dependent transient analyses measure the recovery time back to the equilibrium population size and structure (see example in Figure 1B). Past work examining the dynamics of density-dependent structured population models has focused on the local stability of the carrying capacity, defining reactivity as the propensity of perturbations from equilibrium to grow before decaying back to the stable equilibrium (Caswell, 2019; Caswell and Neubert, 2005; Neubert and Caswell, 1997). This approach, like what we have done here, focuses on perturbations to the system when it is at equilibrium. However, Caswell

(Caswell, 2019, p. 207) notes that the local stability approach is based on the inherent system dynamics, while the indices put forward by Stott and colleagues (Capdevila et al., 2020; Stott et al., 2011) are based on the transient responses to a particular initial condition. Further work will be needed to analyse the transient responses of density-dependent models to perturbations that cause a particular initial condition. Still, we have shown that there is one resilience metric that can be generalised to both density-dependent and density-independent models: recovery time. We found that density-dependent recovery time was nearly always longer than density-independent recovery time, indicating that the non-linear model has a greater probability of long transient periods (Hastings et al., 2018).

In our modelling framework, density dependence and disturbance are separate processes, but it is likely that they interact in natural systems. In a perennial plant population, the impact of density on both vital rates and population growth rate depended on whether the plot had experienced a fire that year or not (Gornish, 2013). For red deer (*Cervus elaphus*) in Scotland, the cessation of culling led to both changes in population density and population structure, resulting in long-term transient dynamics and density-dependent oscillations (Coulson et al., 2004). Transient life table response experiment (LTRE) analysis holds the potential to disentangle the effects of variation in vital rates and variation in population structure (Knape et al., 2023; Koons et al., 2016), such as could result from the interacting effects of density-dependence and disturbance. However, transient LTREs have so far been underutilized, perhaps because fewer than 40% of the publications archived in the COMADRE and COMPADRE databases (a representative sample of published matrix population models) include data on observed population distributions (Gascoigne et al., 2023).

In spite of the idiosyncratic patterns of resilience across densities and life history strategies, a few patterns with life history strategy remain reliable. Specifically, compensation

is greatest and resistance lowest in fast life histories, and vice versa in slow life histories. Additionally, we found that recovery time estimates from the density-independent framework were furthest from the recovery time of the true underlying density-dependent model in virtual species with long generation times and high iteroparity. Therefore, identifying density-dependent effects in more slow-living species, where there are already more conservation concerns (Lande 1998; Purvis et al. 2000, but see Paniw et al. 2018) may be most urgent for predicting responses to disturbance and management intervention. Finally, to truly understand the resilience of natural populations of plants and animals, then we must update transient dynamics methods and the demographic resilience framework to accommodate time-varying vital rates. These advances will substantially improve our ability to predict the responses of species to the myriad and increasingly frequent disturbances they face.

References

Adler, P. B., Smull, D., Beard, K. H., Choi, R. T., Furniss, T., Kulmatiski, A., Meiners, J. M., Tredennick, A. T., & Veblen, K. E. (2018). Competition and coexistence in plant communities: Intraspecific competition is stronger than interspecific competition. *Ecology Letters*, *21*(9), 1319–1329.

Bassar, R. D., López-Sepulcre, A., Walsh, M. R., Turcotte, M. M., Torres-Mejia, M., & Reznick, D. N. (2010). Bridging the gap between ecology and evolution: Integrating density regulation and life-history evolution. *Annals of the New York Academy of Sciences*, *1206*(1), 17–34. https://doi.org/10.1111/j.1749-6632.2010.05706.x

Bienvenu, F., & Legendre, S. (2015). A new approach to the generation time in matrix population models. *American Naturalist*, *185*, 834–843. https://doi.org/10.1086/681104

Bonenfant, C., Gaillard, J.-M., Coulson, T., Festa-Bianchet, M., Loison, A., Garel, M., Loe, L. E., Blanchard, P., Pettorelli, N., Owen-Smith, N., Du Toit, J., & Duncan, P. (2009). Chapter 5 Empirical evidence of density-dependence in populations of large herbivores. In *Advances in Ecological Research* (pp. 313–357, Vol. 41). Elsevier. https://doi.org/10.1016/S0065-2504(09)00405-X

Butchart, S. H., Walpole, M., Collen, B., Van Strien, A., Scharlemann, J. P., Almond, R. E., Baillie, J. E., Bomhard, B., Brown, C., Bruno, J., et al. (2010). Global biodiversity: Indicators of recent declines. *Science*, *328*(5982), 1164–1168.

Cant, J., Reimer, J. D., Sommer, B., Cook, K. M., Kim, S. W., Sims, C. A., Mezaki, T., O'Flaherty, C., Brooks, M., Malcolm, H. A., et al. (2023). Coral assemblages at higher latitudes favor short-term potential over long-term performance. *Ecology*, *104*(9), e4138.

Capdevila, P., Stott, I., Beger, M., & Salguero-Gómez, R. (2020). Towards a comparative framework of demographic resilience. *Trends in Ecology & Evolution*, *35*(9), 776–786. https://doi.org/10.1016/j.tree.2020.05.001

Capdevila, P., Stott, I., Cant, J., Beger, M., Rowlands, G., Grace, M., & Salguero-Gómez, R. (2022). Life history mediates the trade-offs among different components of demographic resilience. *Ecology Letters*. https://doi.org/10.1111/ele.14004

Capdevila, P., Stott, I., Cant, J., Beger, M., Rowlands, G., Grace, M., & Salguero-Gómez, R. (2024). Correction to 'Life history mediates the trade-offs among different components of demographic resilience'. *Ecology Letters*, *27*(7), e14468. https://doi.org/ https://doi.org/10.1111/ele.14468

Caswell, H. (2001). *Matrix population models* (2nd ed.). Sinauer Associates.

Caswell, H. (2019). *Sensitivity analysis: Matrix methods in demography and ecology*. Springer Nature.

Caswell, H., & Neubert, M. G. (2005). Reactivity and transient dynamics of discrete-time ecological systems. *Journal of Difference Equations and Applications*, *11*(4-5), 295–310.

Chesson, P. (2000). Mechanisms of maintenance of species diversity. *Annual review of Ecology and Systematics*, *31*(1), 343–366.

Coulson, T. (2021). We live in a changing world, but that shouldn't mean we abandon the concept of equilibrium. *Ecology Letters*, *24*(1), 3–5. https://doi.org/10.1111/ele.13629

Coulson, T., Catchpole, E. A., Albon, S. D., Morgan, B. J. T., Pemberton, J. M., Clutton-Brock, T. H., Crawley, M. J., & Grenfell, B. T. (2001). Age, sex, density, winter weather, and population crashes in Soay sheep. *Science*, *292*(5521), 1528–1531. https://doi.org/10.1126/science.292.5521.1528

Coulson, T., Guinness, F., Pemberton, J., & Clutton-Brock, T. (2004). The demographic consequences of releasing a population of red deer from culling. *Ecology*, *85*(2), 411–422.

Courchamp, F., Clutton-Brock, T., & Grenfell, B. (1999). Inverse density dependence and the Allee effect. *Trends in ecology & evolution*, *14*(10), 405–410.

Crone, E. E., Menges, E. S., Ellis, M. M., Bell, T., Bierzychudek, P., Ehrlén, J., Kaye, T. N., Knight, T. M., Lesica, P., Morris, W. F., Oostermeijer, G., Quintana-Ascencio, P. F., Stanley, A., Ticktin, T., Valverde, T., & Williams, J. L. (2011). How do plant ecologists use matrix population models? *Ecology Letters*, *14*(1), 1–8. https://doi.org/10.1111/j.1461-0248.2010.01540.x

Csergő, A. M., Salguero-Gómez, R., Broennimann, O., Coutts, S. R., Guisan, A., Angert, A. L., Welk, E., Stott, I., Enquist, B. J., McGill, B., et al. (2017). Less favourable climates constrain demographic strategies in plants. *Ecology letters*, *20*(8), 969–980.

Demetrius, L. (1977). Measures of fitness and demographic stability. *Proceedings of the National Academy of Sciences*, *74*, 384–386. https://doi.org/10.1073/pnas.74.1.384

Doody, J. S., Green, B., Rhind, D., Castellano, C. M., Sims, R., & Robinson, T. (2009). Population-level declines in Australian predators caused by an invasive species. *Animal Conservation*, *12*(1), 46–53.

Enquist, B. J., Erwin, D., Savage, V., & Marquet, P. A. (2024). Scaling approaches and macroecology provide a foundation for assessing ecological resilience in the Anthropocene. *Philosophical Transactions of the Royal Society B: Biological Sciences*, *379*(1902), 20230010. https://doi.org/10.1098/rstb.2023.0010

Gaillard, J.-M., Yoccoz, N. G., Lebreton, J.-D., Bonenfant, C., Devillard, S., Loison, A., Pontier, D., & Allaine, D. (2005). Generation time: A reliable metric to measure life-history variation among mammalian populations. *The American Naturalist*, *166*(1), 119–123.

Gamelon, M., Gimenez, O., Baubet, E., Coulson, T., Tuljapurkar, S., & Gaillard, J.-M. (2014). Influence of life-history tactics on transient dynamics: A comparative analysis across mammalian populations. *The American Naturalist*, *184*(5), 673–683. https://doi.org/10.1086/677929

Gascoigne, S. J. L., Rolph, S., Sankey, D., Nidadavolu, N., Stell Pičman, A. S., Hernández, C. M., Philpott, M. E. R., Salam, A., Bernard, C., Fenollosa, E., Lee, Y. J., McLean, J., Hetti Achchige Perera, S., Spacey, O. G., Kajin, M., Vinton, A. C., Archer, C. R., Burns, J. H., Buss, D. L., … Salguero-Gómez, R. (2023). A standard protocol to report discrete stage-structured demographic information. *Methods in Ecology and Evolution*, *14*(8), 2065–2083. https://doi.org/10.1111/2041-210X.14164

Gornish, E. S. (2013). Effects of density and fire on the vital rates and population growth of a perennial goldenaster. *AoB PLANTS*, *5*. https://doi.org/10.1093/aobpla/plt041

Hare, J. A., Morrison, W. E., Nelson, M. W., Stachura, M. M., Teeters, E. J., Griffis, R. B., Alexander, M. A., Scott, J. D., Alade, L., Bell, R. J., et al. (2016). A vulnerability assessment of fish and invertebrates to climate change on the northeast US continental shelf. *PloS one*, *11*(2), e0146756.

Hastings, A. (2010). Timescales, dynamics, and ecological understanding. *Ecology*, *91*(12), 3471–3480.

Hastings, A., Abbott, K. C., Cuddington, K., Francis, T., Gellner, G., Lai, Y.-C., Morozov, A., Petrovskii, S., Scranton, K., & Zeeman, M. L. (2018). Transient phenomena in ecology. *Science*, *361*(6406), eaat6412. https://doi.org/10.1126/science.aat6412

Healy, K., Ezard, T. H. G., Jones, O. R., Salguero-Gómez, R., & Buckley, Y. M. (2019). Animal life history is shaped by the pace of life and the distribution of age-specific mortality and reproduction. *Nature Ecology & Evolution*, *3*, 1217–1224. https://doi.org/10.1038/s41559-019-0938-7

Hernández-Yáñez, H., Kim, S. Y., & Che-Castaldo, J. P. (2022). Demographic and life history traits explain patterns in species vulnerability to extinction. *PloS one*, *17*(2), e0263504.

Horvitz, C. C., McMann, S., & Freedman, A. (1995). Exotics and hurricane damage in three hardwood hammocks in Dade County parks, Florida. *Journal of Coastal Research*, 145–158.

Iles, D. T., Salguero-Gómez, R., Adler, P. B., & Koons, D. N. (2016). Linking transient dynamics and life history to biological invasion success. *Journal of Ecology*, *104*(2), 399–408. https://doi.org/10.1111/1365-2745.12516

Ingrisch, J., & Bahn, M. (2018). Towards a comparable quantification of resilience. *Trends in Ecology & Evolution*, *33*(4), 251–259. https://doi.org/10.1016/j.tree.2018.01.013

Jaureguiberry, P., Titeux, N., Wiemers, M., Bowler, D. E., Coscieme, L., Golden, A. S., Guerra, C. A., Jacob, U., Takahashi, Y., Settele, J., Díaz, S., Molnár, Z., & Purvis, A. (2022). The direct drivers of recent global anthropogenic biodiversity loss. *Science Advances*, *8*(45), eabm9982. https://doi.org/10.1126/sciadv.abm9982

Jelbert, K., Buss, D., McDonald, J., Townley, S., Franco, M., Stott, I., Jones, O., Salguero-Gómez, R., Buckley, Y., Knight, T., Silk, M., Sargent, F., Rolph, S., Wilson, P., & Hodgson, D. (2019). Demographic amplification is a predictor of invasiveness among plants. *Nature Communications*, *10*(1), 5602. https://doi.org/10.1038/s41467-019-13556-w

Jones, O. R., Barks, P., Stott, I., James, T. D., Levin, S., Petry, W. K., Capdevila, P., Che-Castaldo, J., Jackson, J., Römer, G., Schuette, C., Thomas, C. C., & Salguero-Gómez, R. (2022). Rcompadre and Rage—two R packages to facilitate the use of the COMPADRE and COMADRE databases and calculation of life-history traits from matrix population models. *Methods in Ecology and Evolution*, *13*(4), 770–781. https://doi.org/https://doi.org/10.1111/2041-210X.13792

Knape, J., Paquet, M., Arlt, D., Kačergytė, I., & Pärt, T. (2023). Partitioning variance in population growth for models with environmental and demographic stochasticity. *Journal of Animal Ecology*, *92*(10), 1979–1991. https://doi.org/10.1111/1365-2656.13990

Koons, D. N., Iles, D. T., Schaub, M., & Caswell, H. (2016). A life-history perspective on the demographic drivers of structured population dynamics in changing environments. *Ecology Letters*, *19*(9), 1023–1031. https://doi.org/10.1111/ele.12628

Lande, R. (1998). Anthropogenic, ecological and genetic factors in extinction and conservation. *Researches on Population Ecology*, *40*, 259–269.

Layton-Matthews, K., Loonen, M. J. J. E., Hansen, B. B., Coste, C. F. D., Sæther, B.-E., & Grøtan, V. (2019). Density-dependent population dynamics of a high Arctic capital breeder, the barnacle goose. *Journal of Animal Ecology*, *88*(8), 1191–1201. https://doi.org/10.1111/1365-2656.13001

Levin, L., Caswell, H., Bridges, T., DiBacco, C., Cabrera, D., & Plaia, G. (1996). Demographic responses of estuarine polychaetes to pollutants: Life table response experiments. *Ecological Applications*, *6*, 1295–1313. https://doi.org/10.2307/2269608

McLauchlan, K. K., Higuera, P. E., Miesel, J., Rogers, B. M., Schweitzer, J., Shuman, J. K., Tepley, A. J., Varner, J. M., Veblen, T. T., Adalsteinsson, S. A., et al. (2020). Fire as a fundamental ecological process: Research advances and frontiers. *Journal of Ecology*, *108*(5), 2047–2069.

Meekins, J. F., & McCarthy, B. C. (2002). Effect of population density on the demography of an invasive plant (*Alliaria petiolata*, Brassicaceae) population in a southeastern Ohio forest. *The American midland naturalist*, *147*(2), 256–278.

Metz, M. R., Sousa, W. P., & Valencia, R. (2010). Widespread density-dependent seedling mortality promotes species coexistence in a highly diverse amazonian rain forest. *Ecology*, *91*(12), 3675–3685.

Neubert, M. G., & Caswell, H. (1997). Alternatives to resilience for measuring the responses of ecological systems to perturbations. *Ecology*, *78*(3), 653–665.

Neubert, M. G., & Caswell, H. (2000). Density-dependent vital rates and their population dynamic consequences. *Journal of Mathematical Biology*, *41*(2), 103–121. https://doi.org/10.1007/s002850070001

Oli, M. K., Slade, N. A., & Dobson, F. S. (2001). Effect of density reduction on Uinta ground squirrels: Analysis of life table response experiments. *Ecology*, *82*, 1921–1929. https://doi.org/10.1890/0012-9658(2001)082\[1921:EODROU\]2.0.CO;2

Paniw, M., Ozgul, A., & Salguero-Gómez, R. (2018). Interactive life-history traits predict sensitivity of plants and animals to temporal autocorrelation. *Ecology letters*, *21*(2), 275–286.

Paniw, M., Quintana-Ascencio, P. F., Ojeda, F., & Salguero-Gómez, R. (2017). Interacting livestock and fire may both threaten and increase viability of a fire-adapted Mediterranean carnivorous plant. *Journal of Applied Ecology*, *54*(6), 1884–1894. https://doi.org/10.1111/1365-2664.12872

Pearson, R. G., Stanton, J. C., Shoemaker, K. T., Aiello-Lammens, M. E., Ersts, P. J., Horning, N., Fordham, D. A., Raxworthy, C. J., Ryu, H. Y., McNees, J., et al. (2014). Life history and spatial traits predict extinction risk due to climate change. *Nature Climate Change*, *4*(3), 217–221.

Purvis, A., Gittleman, J. L., Cowlishaw, G., & Mace, G. M. (2000). Predicting extinction risk in declining species. *Proceedings of the royal society of London. Series B: Biological Sciences*, *267*(1456), 1947–1952.

R Core Team. (2023). *R: A language and environment for statistical computing*. R Foundation for Statistical Computing. Vienna, Austria. https://www.R-project.org/

Sah, J. P., Ross, M. S., Snyder, J. R., & Ogurcak, D. E. (2010). Tree mortality following prescribed fire and a storm surge event in slash pine (*Pinus elliottii* var. *densa*) forests in the Florida Keys, USA. *International Journal of Forestry Research*, *2010*(1), 204795.

Salguero-Gómez, R. (2017). Applications of the fast–slow continuum and reproductive strategy framework of plant life histories. *New Phytologist*, *213*, 1618–1624. https://doi.org/10.1111/nph.14289

Salguero-Gómez, R., & Casper, B. B. (2010). Keeping plant shrinkage in the demographic loop. *Journal of Ecology*, *98*(2), 312–323.

Salguero-Gómez, R., & Casper, B. B. (2011). A hydraulic explanation for size-specific plant shrinkage: Developmental hydraulic sectoriality. *New Phytologist*, *189*(1), 229–240.

Salguero-Gómez, R., Jones, O. R., Archer, C. R., Bein, C., de Buhr, H., Farack, C., Gottschalk, F., Hartmann, A., Henning, A., Hoppe, G., Römer, G., Ruoff, T., Sommer, V., Wille, J., Voigt, J., Zeh, S., Vieregg, D., Buckley, Y. M., Che-Castaldo, J., ... Vaupel, J. W. (2016a). COMADRE: A global data base of animal demography. *Journal of Animal Ecology*, *85*(2), 371–384. https://doi.org/10.1111/1365-2656.12482

Salguero-Gómez, R., Jones, O. R., Archer, C. R., Buckley, Y. M., Che-Castaldo, J., Caswell, H., Hodgson, D., Scheuerlein, A., Conde, D. A., Brinks, E., Buhr, H., Farack, C., Gottschalk, F., Hartmann, A., Henning, A., Hoppe, G., Römer, G., Runge, J., Ruoff, T., ... Vaupel, J. W. (2015). The COMPADRE plant matrix database: An open online repository for plant demography. *Journal of Ecology*, *103*, 202–218. https://doi.org/10.1111/1365-2745.12334

Salguero-Gómez, R., Jones, O. R., Jongejans, E., Blomberg, S. P., Hodgson, D. J., Mbeau-Ache, C., Zuidema, P. A., Kroon, H. D., & Buckley, Y. M. (2016b). Fast-slow continuum and reproductive strategies structure plant life-history variation worldwide. *Proceedings of the National Academy of Sciences of the United States of America*, *113*, 230–235. https://doi.org/10.1073/pnas.1506215112

Salguero-Gómez, R., & Plotkin, J. B. (2010). Matrix dimensions bias demographic inferences: Implications for comparative plant demography. *The American Naturalist*, *176*(6), 710–722. https://doi.org/10.1086/657044

Santini, L., Isaac, N. J. B., & Ficetola, G. F. (2018). TetraDENSITY: A database of population density estimates in terrestrial vertebrates. *Global Ecology and Biogeography*, *27*(7), 787–791. https://doi.org/10.1111/geb.12756

Sarkar, D. (2008). *Lattice: Multivariate data visualization with R*. Springer. http://lmdvr.r-forge.r-project.org

Sax, D. F., & Brown, J. H. (2000). The paradox of invasion. *Global Ecology and Biogeography*, *9*(5), 363–371. https://doi.org/10.1046/j.1365-2699.2000.00217.x

Scheffer, M., Carpenter, S. R., Dakos, V., & Van Nes, E. H. (2015). Generic indicators of ecological resilience: Inferring the chance of a critical transition. *Annual Review of Ecology, Evolution, and Systematics*, *46*(1), 145–167. https://doi.org/10.1146/annurev-ecolsys-112414-054242

Shepherd, J. G., & Cushing, D. H. (1980). A mechanism for density-dependent survival of larval fish as the basis of a stock-recruitment relationship. *ICES Journal of Marine Science*, *39*(2), 160–167. https://doi.org/10.1093/icesjms/39.2.160

Stearns, S. C. (1977). The evolution of life history traits: A critique of the theory and a review of the data. *Annual Review of Ecology and Systematics*, *8*(1), 145–171. https://doi.org/10.1146/annurev.es.08.110177.001045

Stott, I., Hodgson, D. J., & Townley, S. (2012). Popdemo: An R package for population demography using projection matrix analysis. *Methods in Ecology and Evolution*, *3*(5), 797–802. https://doi.org/10.1111/j.2041-210X.2012.00222.x

Stott, I., Townley, S., & Hodgson, D. J. (2011). A framework for studying transient dynamics of population projection matrix models. *Ecology Letters*, *14*(9), 959–970. https://doi.org/10.1111/j.1461-0248.2011.01659.x

Takada, T., & Nakashizuka, T. (1996). Density-dependent demography in a Japanese temperate broad-leaved forest. *Vegetatio*, *124*(2), 211–221. https://doi.org/10.1007/BF00045495

Turner, M. G. (2010). Disturbance and landscape dynamics in a changing world. *Ecology*, *91*(10), 2833–2849.

Urban, M. C. (2015). Accelerating extinction risk from climate change. *Science*, *348*(6234), 571–573.

White, J. W., Rassweiler, A., Samhouri, J. F., Stier, A. C., & White, C. (2014). Ecologists should not use statistical significance tests to interpret simulation model results. *Oikos*, *123*(4), 385–388. https://doi.org/10.1111/j.1600-0706.2013.01073.x

Wikelski, M., & Thom, C. (2000). Marine iguanas shrink to survive El Niño. *Nature*, *403*(6765), 37–38.

Williams, J. L., Ellis, M. M., Bricker, M. C., Brodie, J. F., & Parsons, E. W. (2011). Distance to stable stage distribution in plant populations and implications for near-term population projections. *Journal of Ecology*, *99*(5), 1171–1178. https://doi.org/10.1111/j.1365-2745.2011.01845.x

Wills, C., Condit, R., Foster, R. B., & Hubbell, S. P. (1997). Strong density- and diversity-related effects help to maintain tree species diversity in a neotropical forest. *Proceedings of the National Academy of Sciences*, *94*(4), 1252–1257. https://doi.org/10.1073/pnas.94.4.1252

Section S1 Model tuning for density dependence

For each scenario, we solved analytically for per-capita reproductive output (ϕ) or maximum per-capita reproductive output (ϕ_{max}) value that corresponds to the population model having its equilibrium population size ('carrying capacity') at a density of 1. Density is calculated as a simple sum of the number of juveniles and adults ($N(t) = n_j(t) + n_a(t)$).

The method for solving for ϕ or ϕ_{max} is as follows:

A. Write the population projection matrix with one vital rate as a function of density, following the form $r(N) = r_{max}e^{-bN}$.

B. Solve for the equilibrium population distribution for juveniles $\hat{n}_j$ and adults $\hat{n}_a$ that are unchanged by projection to the next time step.

C. Set $\hat{n}_j + \hat{n}_a = 1$ and solve for ϕ (or ϕ_{max} in the case where ϕ is the density-dependent vital rate).

The analytical solutions are as follows:

Density-dependent juvenile survival

$$\phi = \frac{\left[1 - (1-\gamma)\sigma_{j,max}e^{-b}\right]\left[(1-\gamma) - \sigma_a(1-\rho)(1-\gamma)\right]}{\gamma(1-\gamma)\sigma_{j,max}e^{-b}} - \sigma_a\rho \tag{S1}$$

Density-dependent progression

$$\phi = \frac{-1}{\sigma_j\gamma_{max}e^{-b}}\left[\sigma_a\rho(\sigma_j - 1) + (\sigma_a - 1)\left(1 - \sigma_j(1 - \gamma_{max}e^{-b})\right)\right] \tag{S2}$$

Density-dependent adult survival

$$\phi = \frac{1 - \sigma_j(1-\gamma) - \sigma_{a,max} e^{-b} \left[\sigma_j \gamma \rho + (1-\rho)(1 - \sigma_j(1-\gamma))\right]}{\sigma_j \gamma} \tag{S3}$$

Density-dependent retrogression

$$\phi = \frac{1}{\sigma_j \gamma} \left[(1-\sigma_a)\left(1 - \sigma_j(1-\gamma)\right) - \sigma_a \rho_{max} \ln 2(\sigma_j - 1)\right] \tag{S4}$$

Density-dependent reproductive output

$$\phi_{max} = e^b \left(\frac{\left[1 - \sigma_j(1-\gamma)\right]\left[1 - \sigma_a(1-\rho)\right]}{\sigma_j \gamma} - \sigma_a \rho \right) \tag{S5}$$

Section S2 Selecting virtual species

We subsetted the COMADRE Animal Matrix Database (Salguero-Gómez et al., 2016) and the COMPADRE Plant Matrix Database (Salguero-Gómez et al., 2015) to matrix population models that are ergodic, irreducible, and primitive. Doing so guarantees the existence of a single dominant eigenvalue (Caswell, 2001, pp. 83-85). We imposed a series of selection criteria on the 3,488 matrix population models available in COMADRE (v. 4.23.3.1) and 8,994 models in COMPADRE (v. 6.23.5.0) to ensure fair comparisons. The criteria are as follows: We retained only models (1) built from demographic data on *both* survival and reproduction, so complete life-cycle information was available; (2) collected in observational ("wild", *i.e.*, non-laboratory) settings without experimental manipulations so the models would reflect the dynamics of natural populations; and (3) published and digitized such that survival and reproduction are separable (*i.e.*, there are separate **F** and **U** matrices). The latter criterion is particularly necessary here to separate the proportion of the matrix element $a_{1,2}$ that corresponds to reproductive output *vs.* to (potentially)

retrogression. Finally, (5) we excluded models with clonal reproduction because permitting fair comparisons between studies with and without clonal reproduction requires careful consideration of ramet *vs.* genet dynamics (Janovský and Herben, 2020) and their emergent vital rates (Salguero-Gómez, 2018). As such, in our virtual species model, we also do not include clonal reproduction.

For each matrix population model that met our criteria, we coerced it into the same model formulation as Equation 1, that is, a two stage model. When models are digitized for the databases, each stage of the model is identified as a propagule, an active member of the population, or a dormant member of the population. Based on the non-zero columns of the fertility ($\mathbf{F}$) matrix, we can also identify each life stage as reproductive or non-reproductive. With the columns of the fertility ($\mathbf{F}$) and survival-growth ($\mathbf{U}$) matrices correctly identified, we can collapse the models down into a 2×2 matrix model matching Equation 1 (Salguero-Gómez and Plotkin, 2010). This last step was performed using the `mpm_collapse` function in the `Rage` package (Jones et al., 2022) in the R programming language.

We then eliminated any collapsed models with incorrect survival values (σ_j or σ_a >1). Finally, we restricted our set of observed models to those with a population growth rate (λ, the dominant eigenvalue of the projection matrix) between 1.0 and 1.6. We chose this range as a realistic comparison with our density-dependent models: at equilibrium ("carrying capacity"), our virtual species models will have $\lambda = 1$ and in early tests of the density-dependent reproductive output case, the highest population growth (at $N \to 0$) was $\lambda \approx 1.6$. Finally, we removed models with extremely high or extremely low reproductive output, with outliers defined as values for ϕ that fall outside of the interval $[LQ - 1.5 * IQR, UQ + 1.5 * IQR]$, where LQ is the lower quartile, UQ is the upper quartile, and IQR is the interquartile range. This final step resulted in a matrix population model for 410 animal, 872 plant, and three fungi populations, representing 100, 204, and one species,

respectively (Supplemental Materials Table S4).

With our final filtered set of collapsed population models, we used a principal components analysis (PCA) to define the space of 'observed life history strategies' (Figure S3). This two-dimensional space captured 70% of the variation among models from COMADRE and COMPADRE (PC1: 43.83%; PC2: 26.25%). PC1 was primarily explained by variation in survival (σ_j, σ_a) and progression (γ), such that longer-lived and late-maturing species score positively on PC1, while short-lived and fast-maturing species score negatively. PC2 was primarily influenced by reproductive output (ϕ), such that species with high reproductive output score positively on PC2 (Supplemental Table S1). As such, we refer to virtual species that fall in the upper left quadrant (low scores on PC1 and high scores on PC2) as exhibiting fast life histories, and we refer to those that fall in the lower right quadrant (high scores on PC1 and low scores on PC2) as exhibiting slow life histories.

To define our virtual species, we inspected the distribution of empirical values of vital rates in our final set of 1,285 collapsed two-stage models. Based on these distributions, we selected a high and low value for adult survival (σ_a), juvenile survival (σ_j), and progression (γ) (Table S2). For retrogression (ρ), we set the low value as 0 (no retrogression at all), and we set our high value near the mean of empirical values in models from the databases where retrogression was greater than 0 (Table S2). We then projected our virtual species models across density-dependent scenarios onto the PC axes as defined by the empirical models. Our virtual species models cover the space of naturally observed populations reasonably well (Supplemental Figure S3). Based on our model scaling, for some virtual species and density-dependent vital rate scenarios, the virtual species plotted at much higher values of PC2 than seen in the empirical models (Supplemental Figure S4). For plotting and analyses, we restricted the virtual species to combinations of vital rates and density-dependent scenarios that had a score on PC2 of ≤ 5.1 for population densities

between 0 and 1.

As these two axes together explain a sufficient amount of variation (>70%), we used these two components to visualize the space occupied by the different life history strategies, as well as to describe how the resilience components of our virtual species are influenced by vital rates and the PC axes (Supplemental Table S3).

Supplemental References

Caswell, H. (2001). *Matrix population models* (2nd ed.). Sinauer Associates.

Janovský, Z., & Herben, T. (2020). Reaching similar goals by different means – differences in life-history strategies of clonal and non-clonal plants. *Perspectives in Plant Ecology, Evolution and Systematics*, *44*, 125534. https://doi.org/https://doi.org/10.1016/j.ppees.2020.125534

Jones, O. R., Barks, P., Stott, I., James, T. D., Levin, S., Petry, W. K., Capdevila, P., Che-Castaldo, J., Jackson, J., Römer, G., Schuette, C., Thomas, C. C., & Salguero-Gómez, R. (2022). Rcompadre and Rage—two R packages to facilitate the use of the COMPADRE and COMADRE databases and calculation of life-history traits from matrix population models. *Methods in Ecology and Evolution*, *13*(4), 770–781. https://doi.org/https://doi.org/10.1111/2041-210X.13792

Salguero-Gómez, R. (2018). Implications of clonality for ageing research. *Evolutionary Ecology*, *32*, 9–28.

Salguero-Gómez, R., Jones, O. R., Archer, C. R., Bein, C., de Buhr, H., Farack, C., Gottschalk, F., Hartmann, A., Henning, A., Hoppe, G., Römer, G., Ruoff, T., Sommer, V., Wille, J., Voigt, J., Zeh, S., Vieregg, D., Buckley, Y. M., Che-Castaldo, J., ... Vaupel, J. W. (2016). COMADRE: A global data base of animal demogra-

phy. *Journal of Animal Ecology*, *85*(2), 371–384. https://doi.org/10.1111/1365-2656.12482

Salguero-Gómez, R., Jones, O. R., Archer, C. R., Buckley, Y. M., Che-Castaldo, J., Caswell, H., Hodgson, D., Scheuerlein, A., Conde, D. A., Brinks, E., Buhr, H., Farack, C., Gottschalk, F., Hartmann, A., Henning, A., Hoppe, G., Römer, G., Runge, J., Ruoff, T., ... Vaupel, J. W. (2015). The COMPADRE plant matrix database: An open online repository for plant demography. *Journal of Ecology*, *103*, 202–218. https://doi.org/10.1111/1365-2745.12334

Salguero-Gómez, R., & Plotkin, J. B. (2010). Matrix dimensions bias demographic inferences: Implications for comparative plant demography. *The American Naturalist*, *176*(6), 710–722. https://doi.org/10.1086/657044

Section S3 Supplemental Figures and Tables

Table S1: The contribution of each vital rate to the first two principal component axes (PC1 and PC2). Loadings in bold indicate a high contribution (greater than ±0.50) of the life-history trait to the PC axis.

Vital rate	Symbol	PC1	PC2
Juvenile survival	σ_j	**0.579**	0.269
Progression	γ	**-0.529**	-0.408
Adult survival	σ_a	**0.569**	0.123
Retrogression	ρ	0.094	0.450
Reproductive output	ϕ	-0.230	**0.735**
Proportion of variance		0.438	0.263
Cumulative proportion of variance		0.438	0.701

Table S2: Empirical and modelled values of vital rates. Empirical values come from the matrix population models from the COMADRE and COMPADRE databases (model selection and vital rate estimation is described in Appendix Section S2). Based on inspection of the distribution of empirical values, we selected the high and low values for each vital rate as seen here.

	Empirical models		**Virtual species**	
Parameter	Mean	Std. dev.	Low value	High value
σ_j	0.66	0.28	0.4	0.9
γ*	0.34	0.35	0.1	0.9
σ_a	0.84	0.23	0.6	0.95
ρ**	0.23	0.25	0	0.3

* The empirical distribution of values for γ was bimodal with values close to 0 and 1 being more common than intermediate values.
** The empirical mean and standard deviation for ρ were calculated for only models where some retrogression was observed ($\rho > 0$).

Table S3: The effects of vital rates and principal component axes on the resilience metrics of compensation, resistance, and recovery time in our virtual species. For each resilience metric, we fit two separate regression models. First, we fit a linear regression with strictly additive terms for each vital rate. Second, we fit a linear regression for the principal component axes including additive terms and their interaction.

Vital rate	Symbol	Regression coefficient		
		Compensation	Resistance	Recovery Time
Juvenile survival	σ_j	-0.402	0.838	-3.679
Progression	γ	-0.351	-0.085	0.588
Adult survival	σ_a	0.626	-0.076	-4.689
Retrogression	ρ	0.152	0.048	2.687
Reproductive output	ϕ	0.771	-0.036	0.201
PC axis 1		-0.094	0.135	-0.805
PC axis 2		0.604	-0.060	-0.383
Interaction PC1 and PC2		-0.023	0.002	-0.705

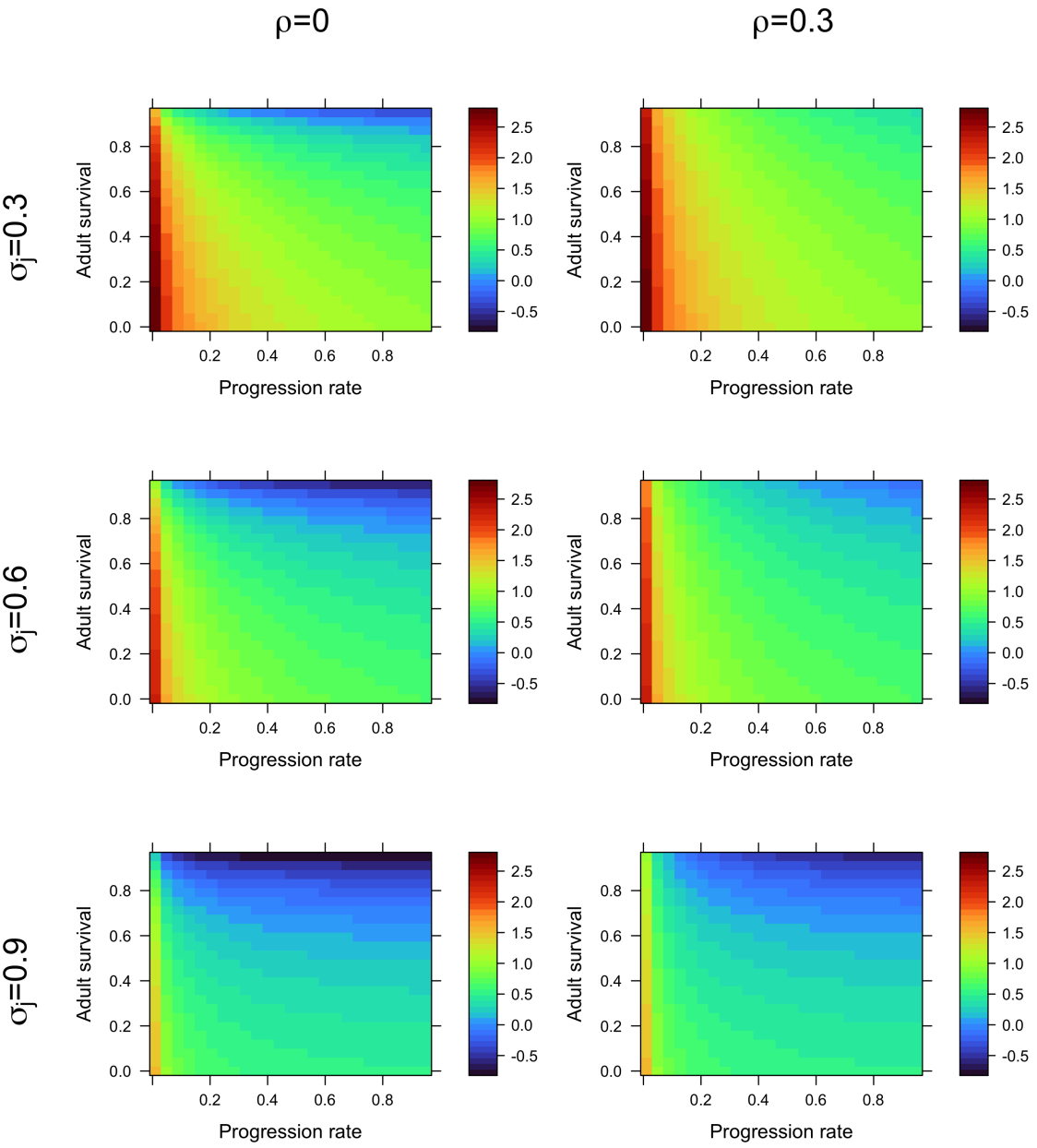

Figure S1: An example of how our model scaling affects maximum reproductive output (ϕ_{max}) across other vital rates. In this case, reproductive output is density-dependent, and the model is scaled such that the population is at its carrying capacity ($\lambda = 1$) when population density ($n_a + n_j$) is equal to 1. In each panel, we show how ϕ_{max} varies across progression (γ) and adult survival (σ_a) for a given value of juvenile survival (σ_j) and retrogression (ρ). The color scales are $\log_{10}(\phi_{max})$.

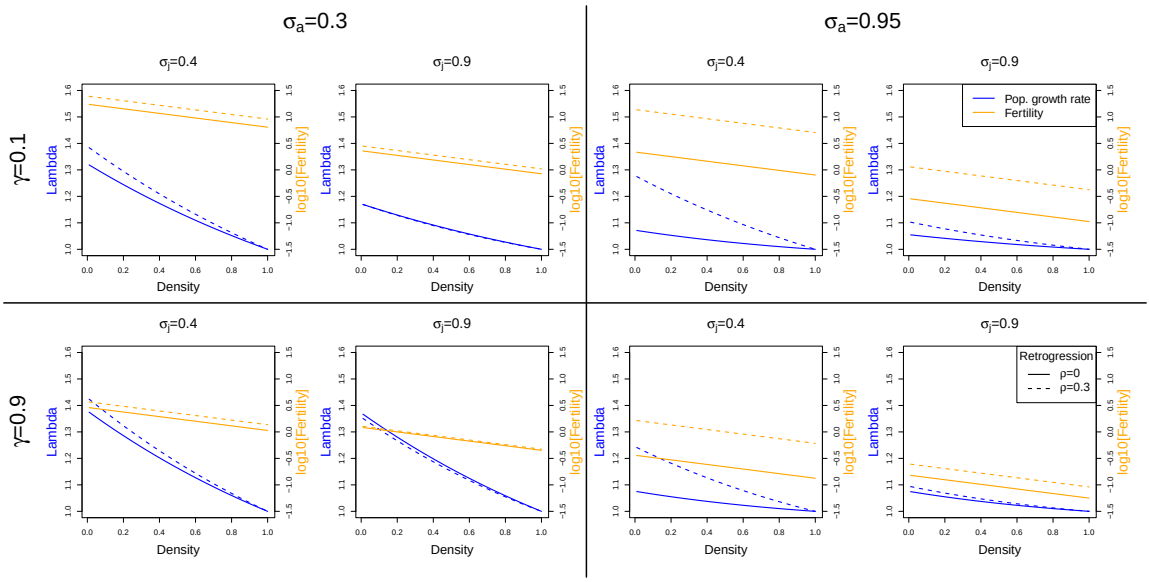

Figure S2: Population growth rate (λ) and per-capita reproductive output (ϕ) across population density for 16 virtual species models.

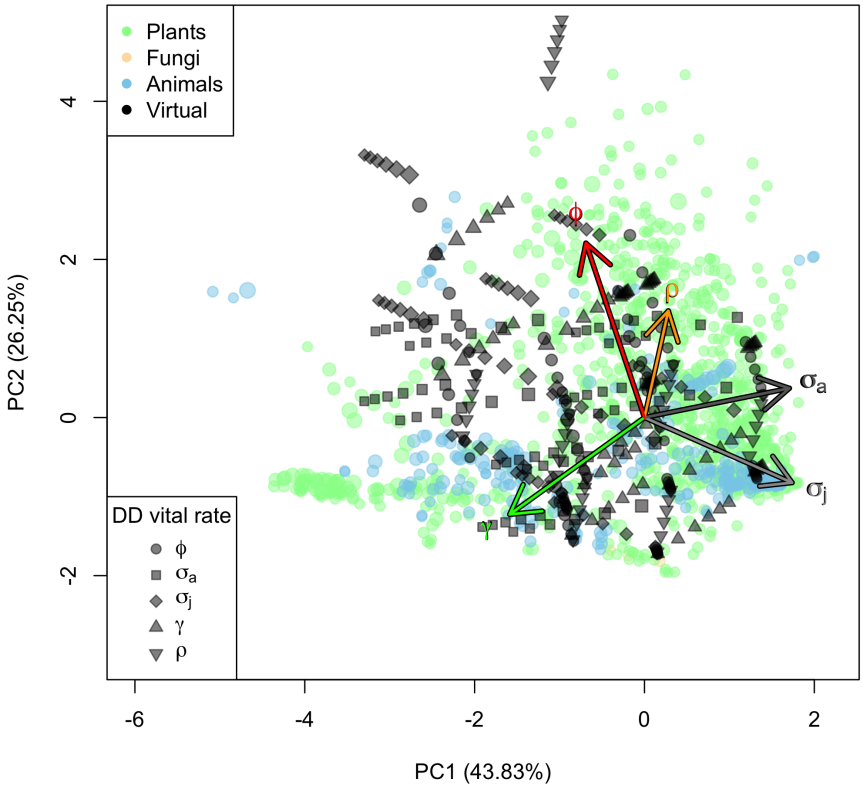

Figure S3: Principal component analysis (PCA) of life history strategies based on the two-stage population model given in Equation 1. The parameters are: juvenile survival (σ_j), juvenile progression (γ), adult survival (σ_a), adult retrogression (ρ), and reproductive output (ϕ). The PCA space is defined by the observed models (colored circles, sized according to their asymptotic population growth rate, λ). The virtual species, shown in black, were then projected onto the PCA space. Each virtual species was modelled with density-dependence on each of the five vital rates (shown with different shapes), and each density-dependent scenario was plotted for six values of density between 0 and 1, sized according to λ. Note that this figure excludes values of PC2 >5.1.

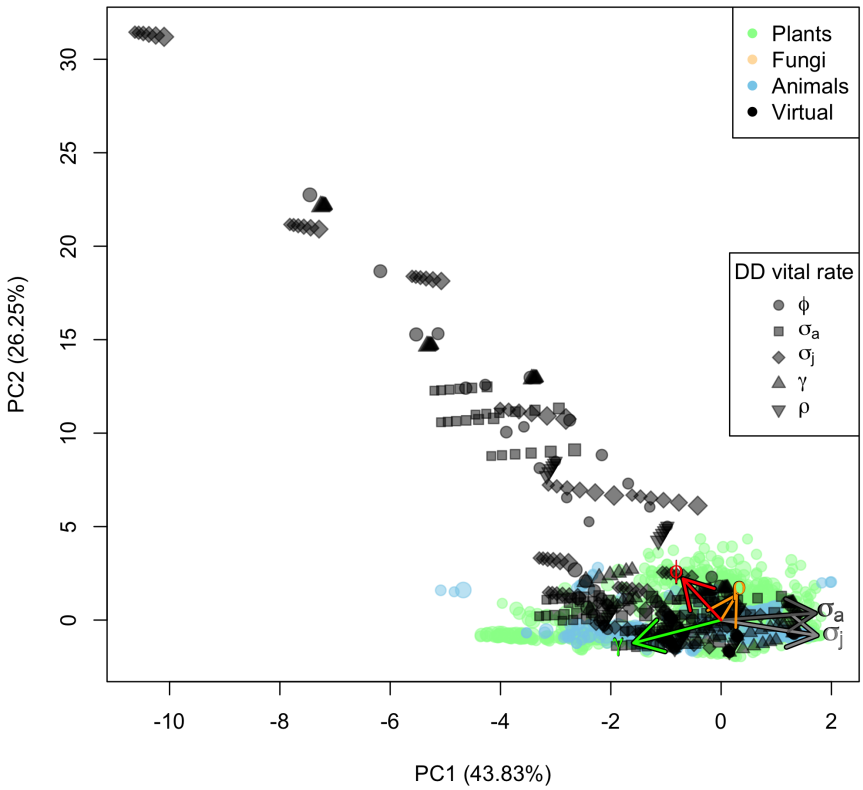

Figure S4: Some of the virtual species and density-dependent vital rate scenarios corresponded to extreme values of PC2, falling far from the space defined by empirical models. Figure details are the same as in Figure S3.

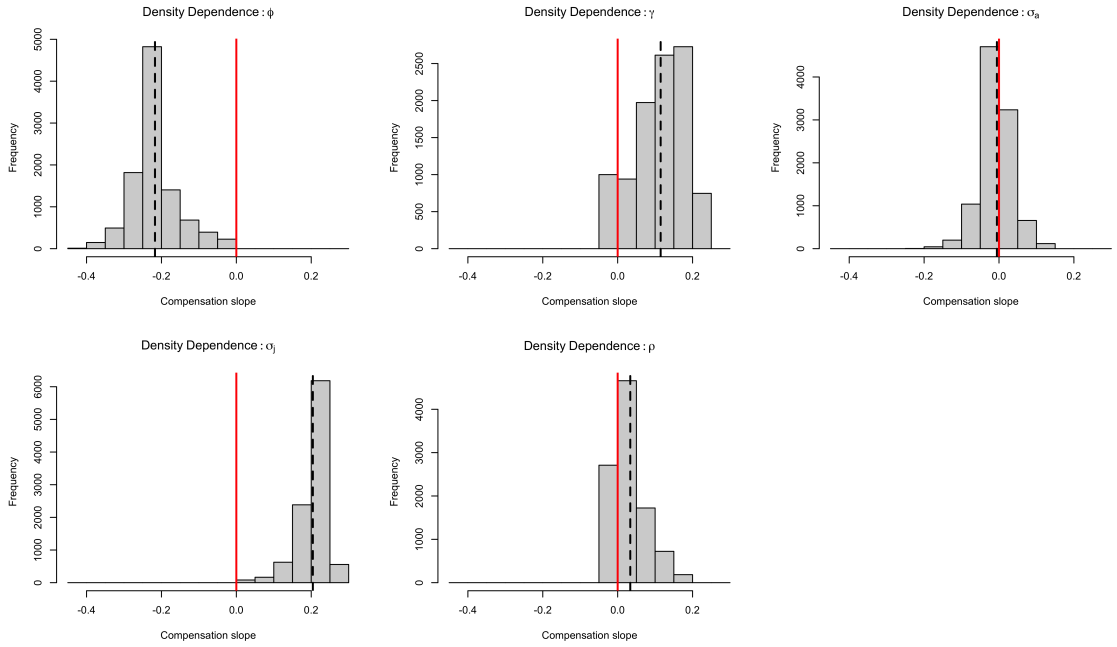

Figure S5: The distribution of compensation slope values depends on which vital rate is the target of density dependence. For each density-dependence scenario, we calculated the slope of compensation across densities (*i.e.*, a in $\log_{10}(C) = a * N + b$, where N is population density and C is the compensation of the population projection matrix calculated at each value of N) for the full range of possible vital rates: $\sigma_j \in [0.01, 1]$; $\gamma \in [0.01, 0.95]$; $\sigma_a \in [0, 0.95]$; and $\rho \in [0, 1]$. For each vital rate, we calculated slopes at 10 values, yielding a total of 10^4 vital rate combinations for each density-dependence scenario. In each panel, a slope of 0 is highlighted with a solid red line, and the mean value of slopes across all tested vital rate combinations is shown with a thick vertical dashed line.

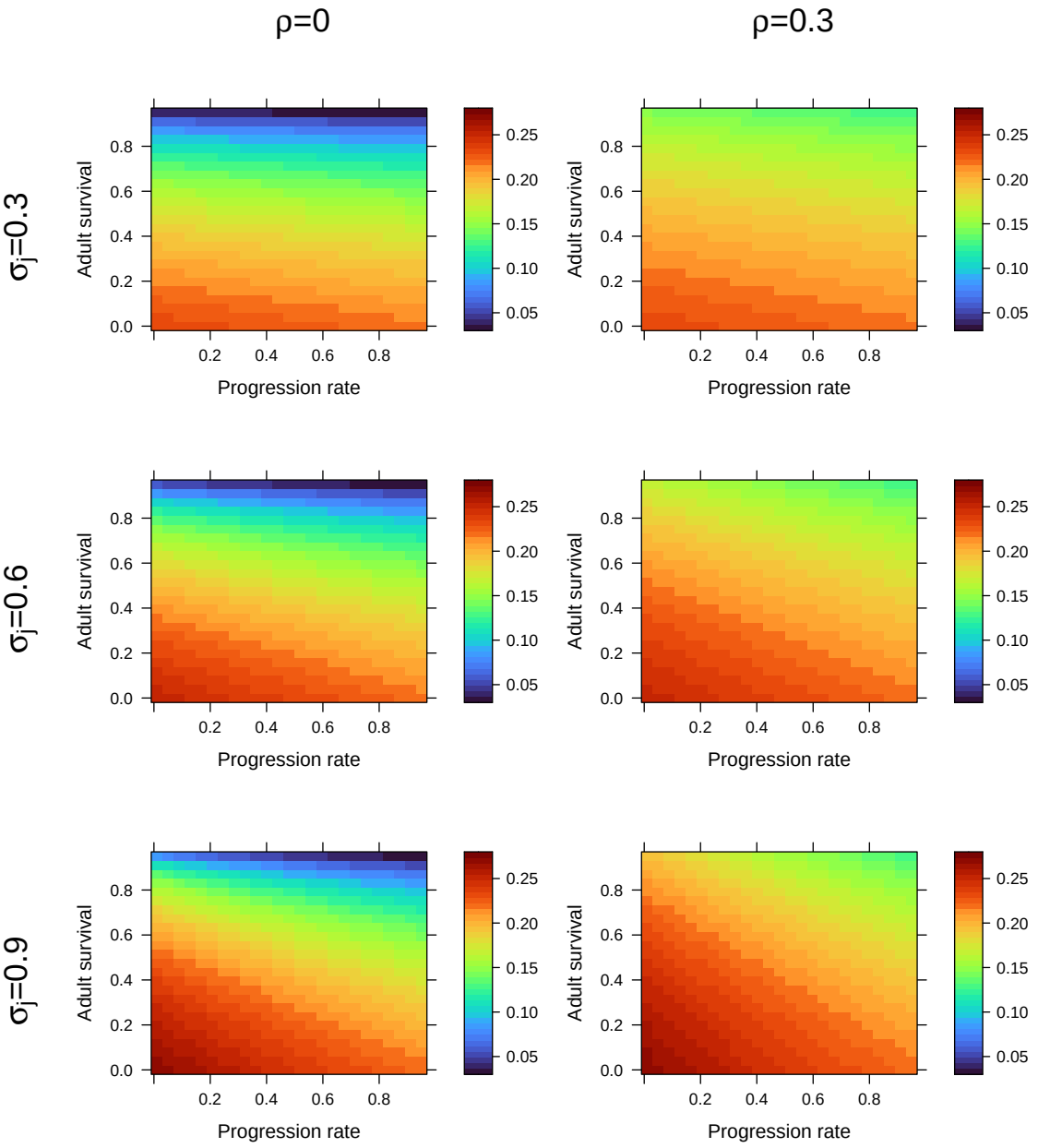

Figure S6: Strength of density effects on compensation when juvenile survival is density-dependent. We calculated the slope of compensation across population densities ($\log C \sim N_t$) for many possible parameter combinations across: $\sigma_a \in [0, 0.95]$, $\gamma \in [0.01, 0.95]$, $\sigma_j = 0.3, 0.6, 0.9$, and $\rho = 0, 0.3$. A single color scale is used for all panels. Slow life histories are in the upper left of each panel, and fast life histories are in the lower right.

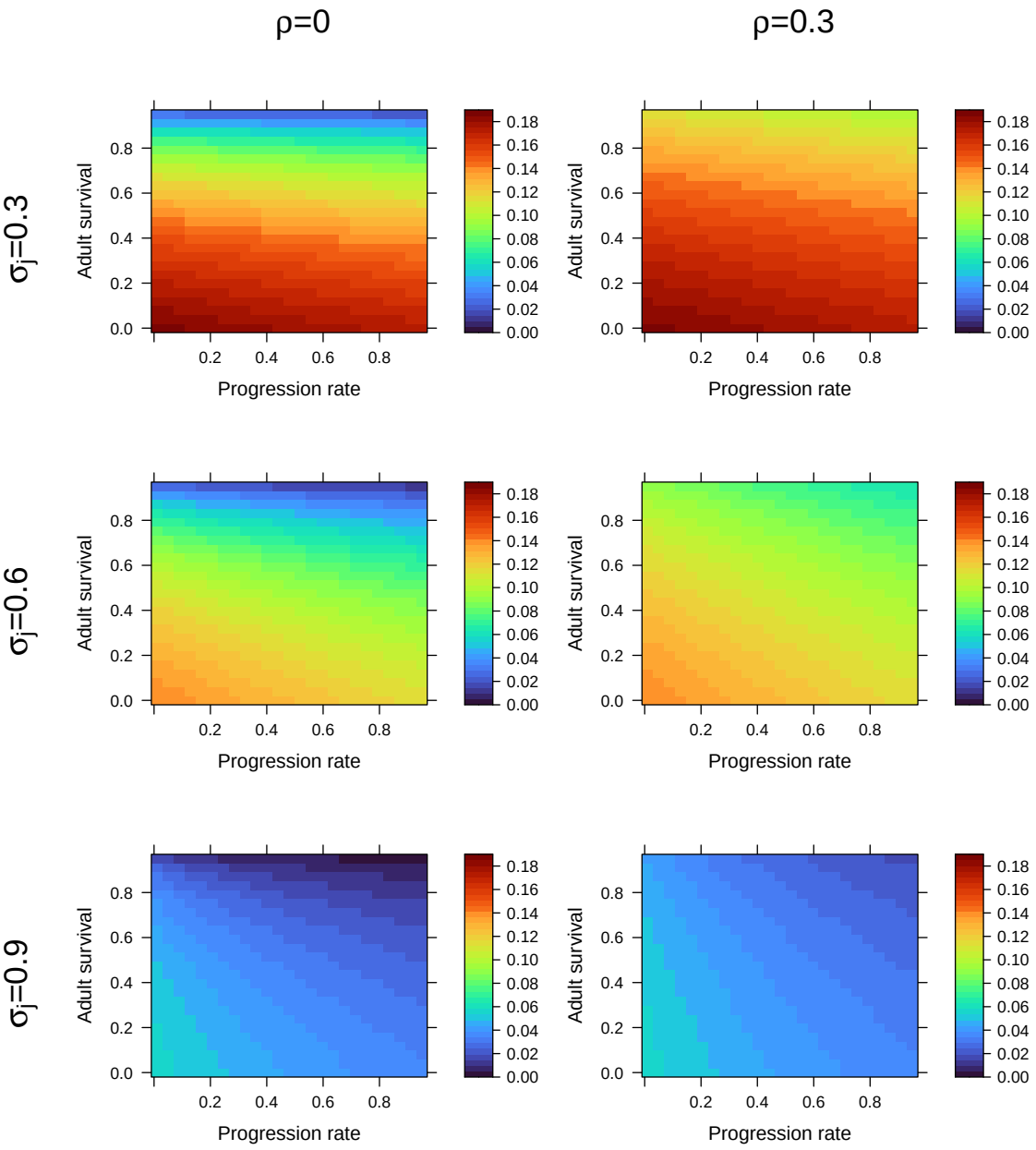

Figure S7: Strength of density effects on compensation when juvenile progression rate is density-dependent. Details are the same as Figure S6.

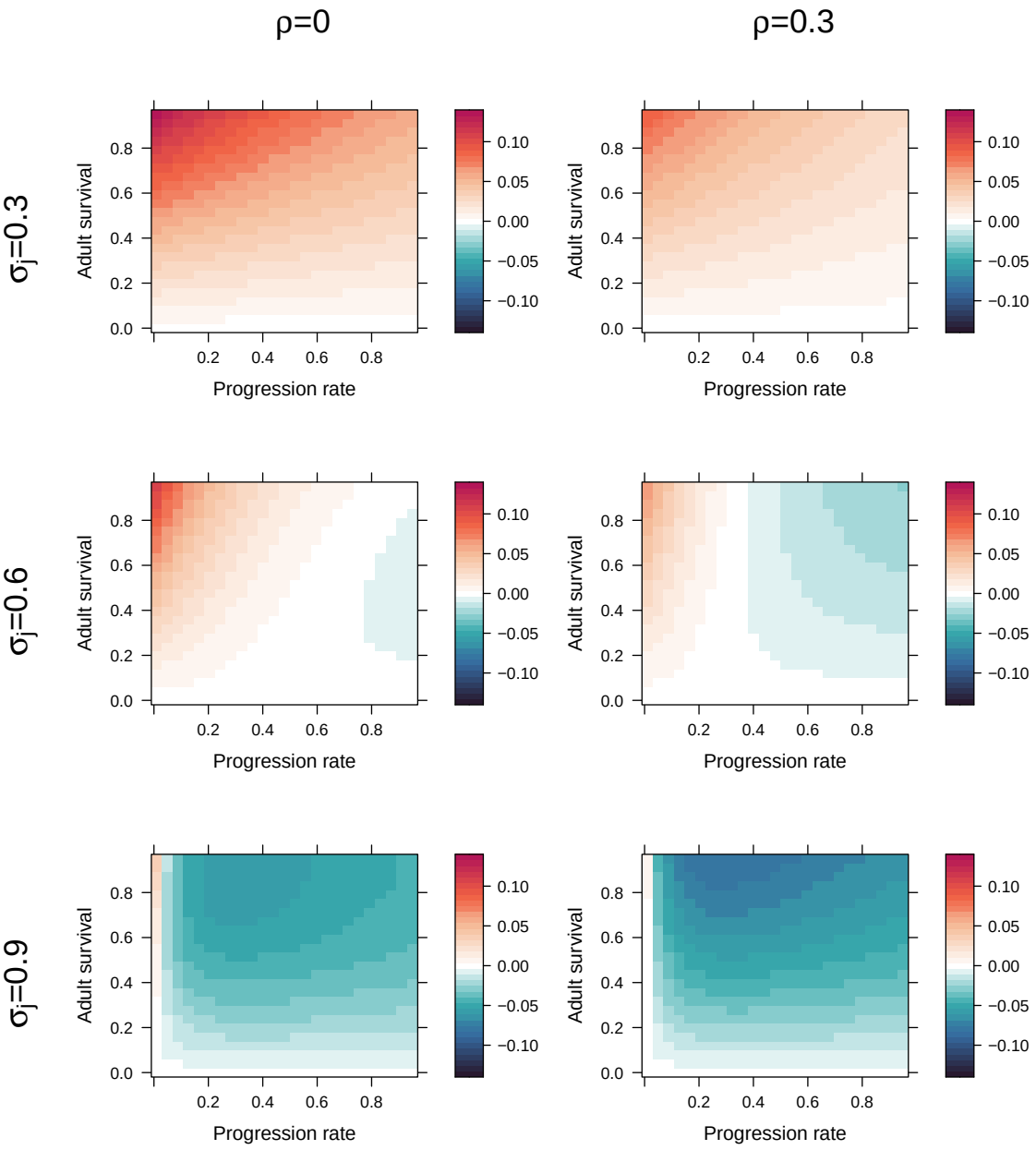

Figure S8: Strength of density effects on compensation when adult survival is density-dependent. Details are the same as Figure S6.

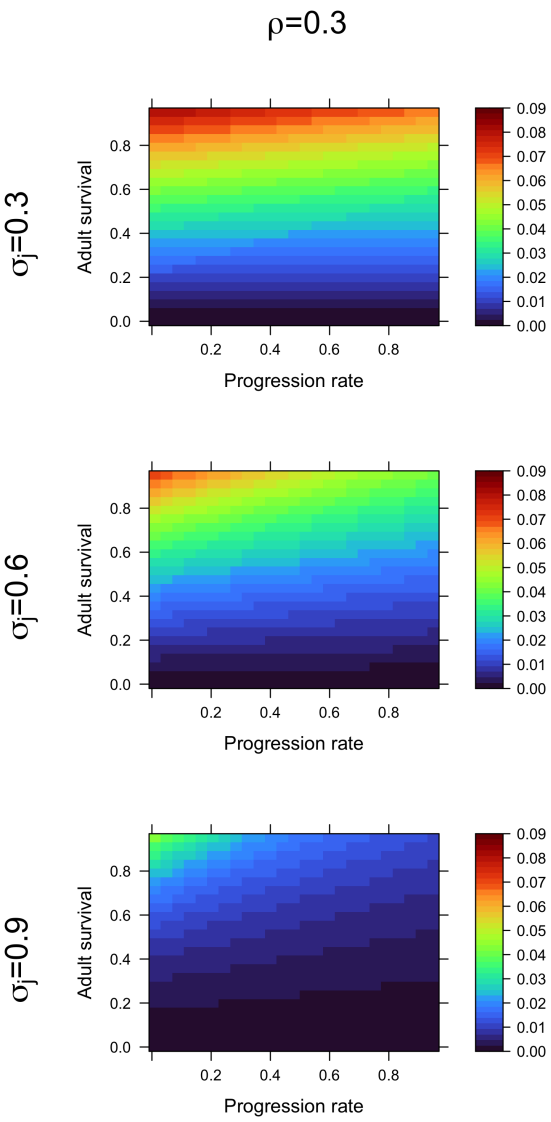

Figure S9: Strength of density effects on compensation when retrogression rate is density-dependent. Details are the same as Figure S6.

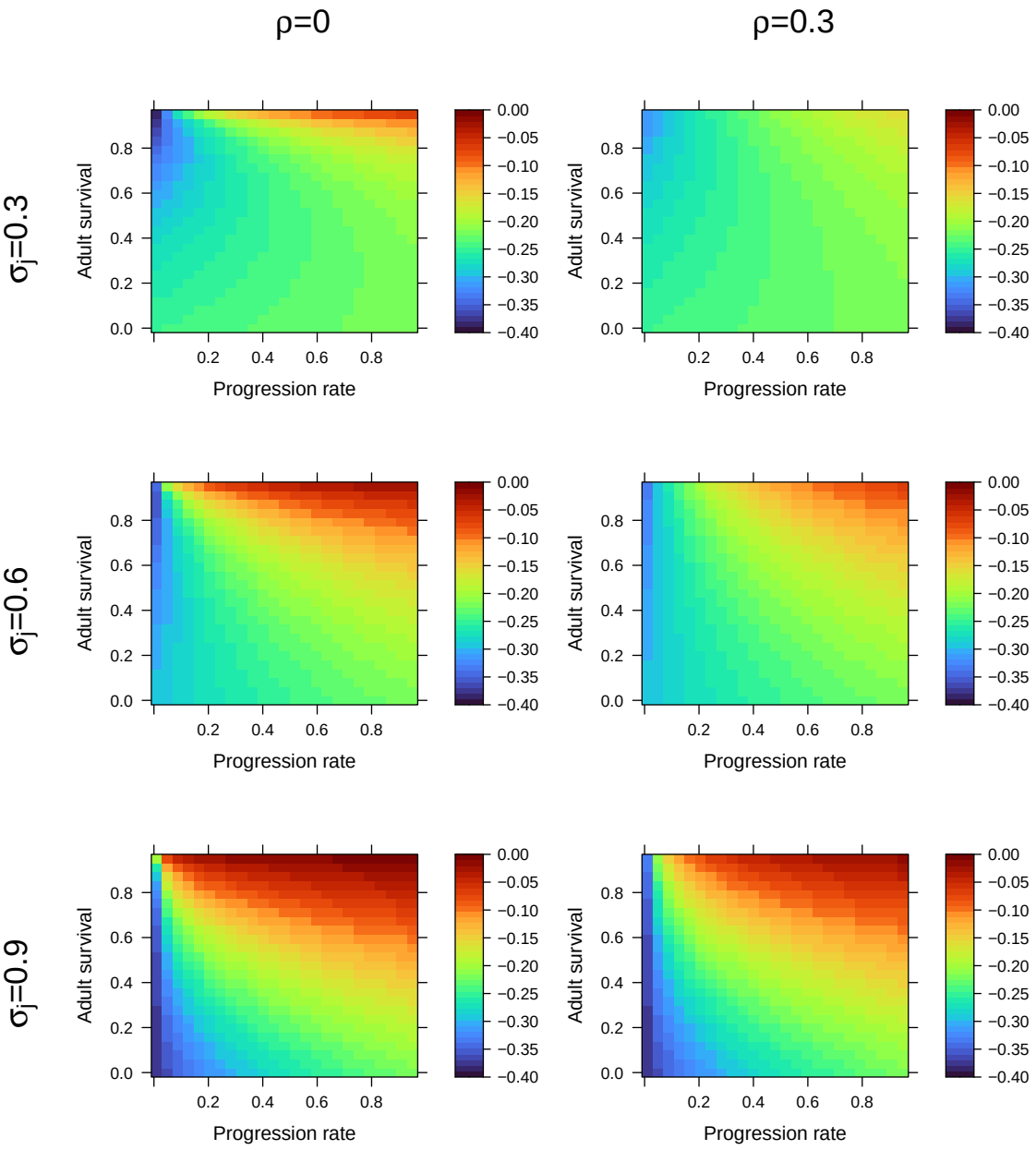

Figure S10: Strength of density effects on compensation when reproductive output is density-dependent. Details are the same as Figure S6.

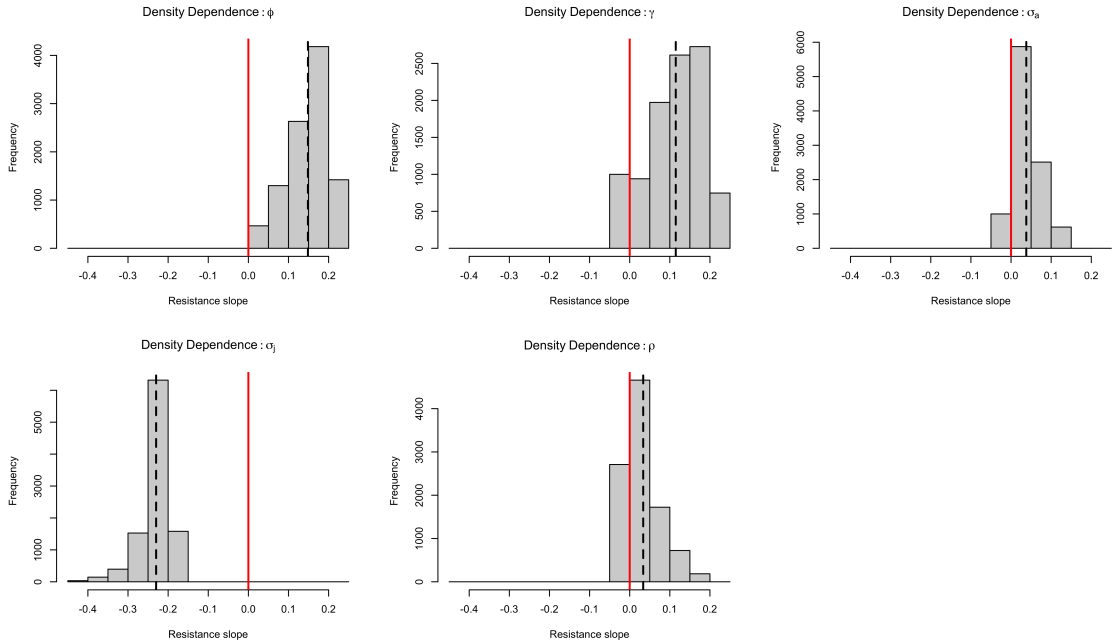

Figure S11: The distribution of resistance slope values depends on which vital rate is the target of density dependence. Details are the same as in Figure S5.

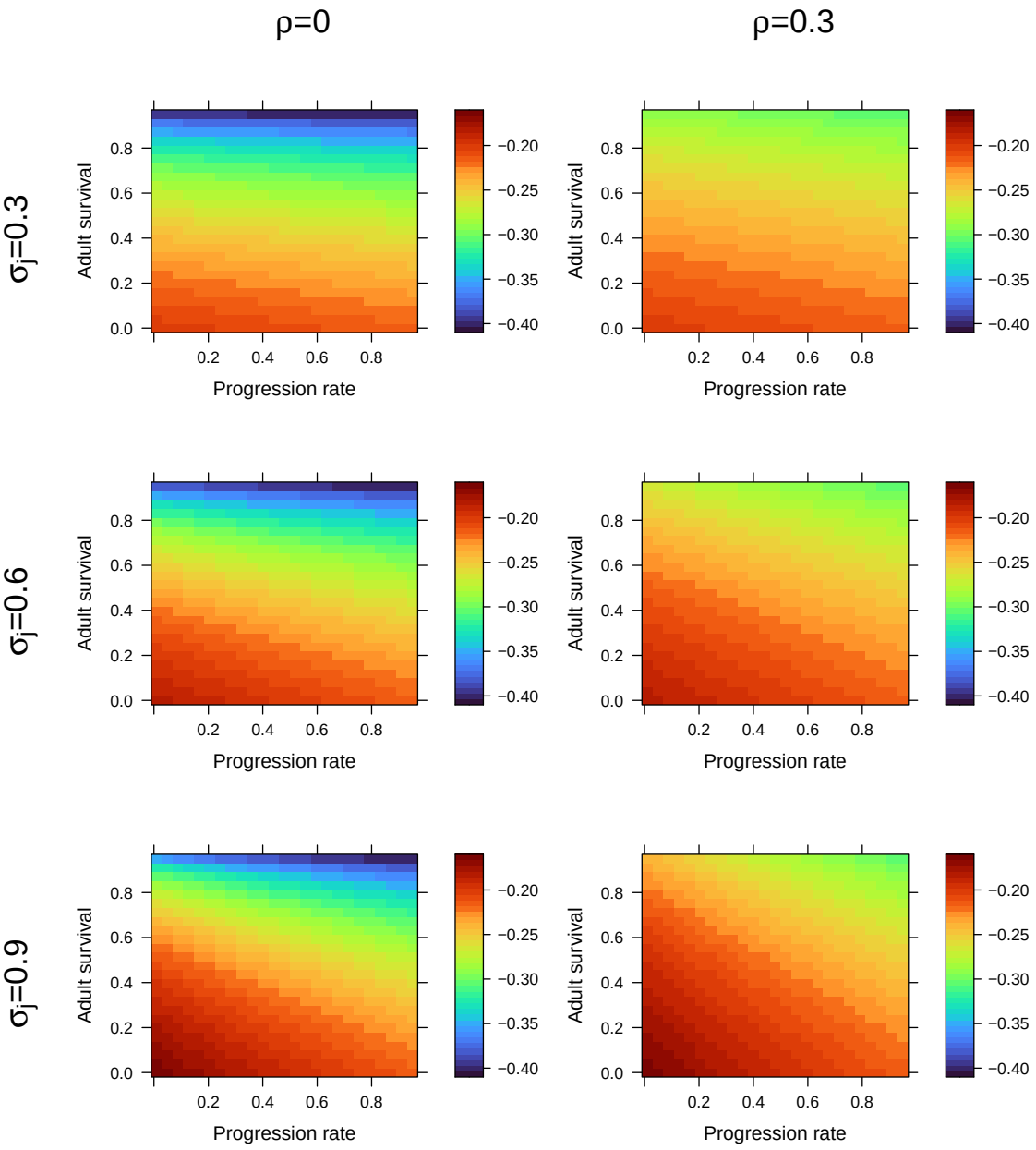

Figure S12: Strength of density effects on resistance when juvenile survival is density-dependent. Details are the same as Figure S6.

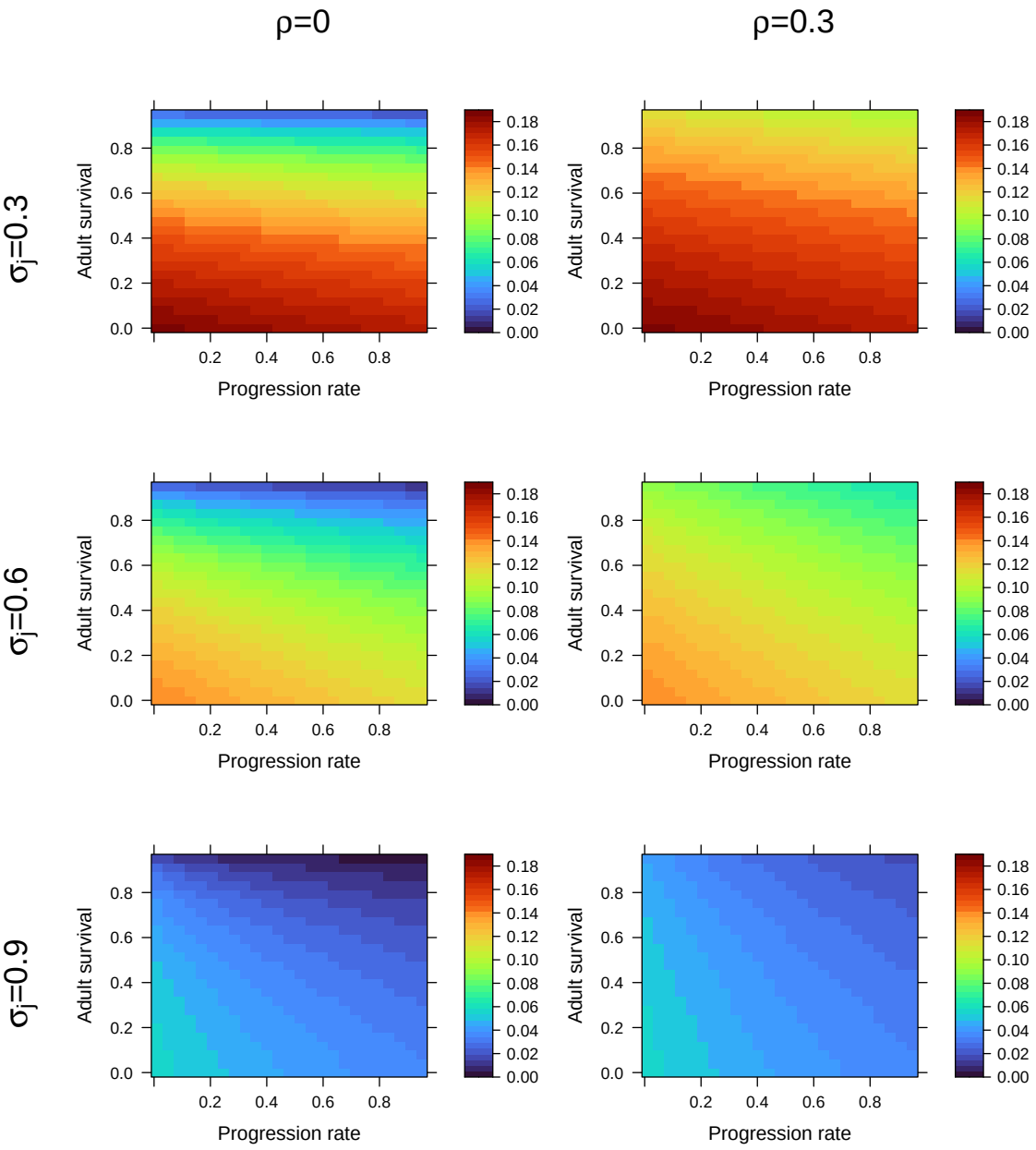

Figure S13: Strength of density effects on resistance when juvenile progression rate is density-dependent. Details are the same as Figure S6.

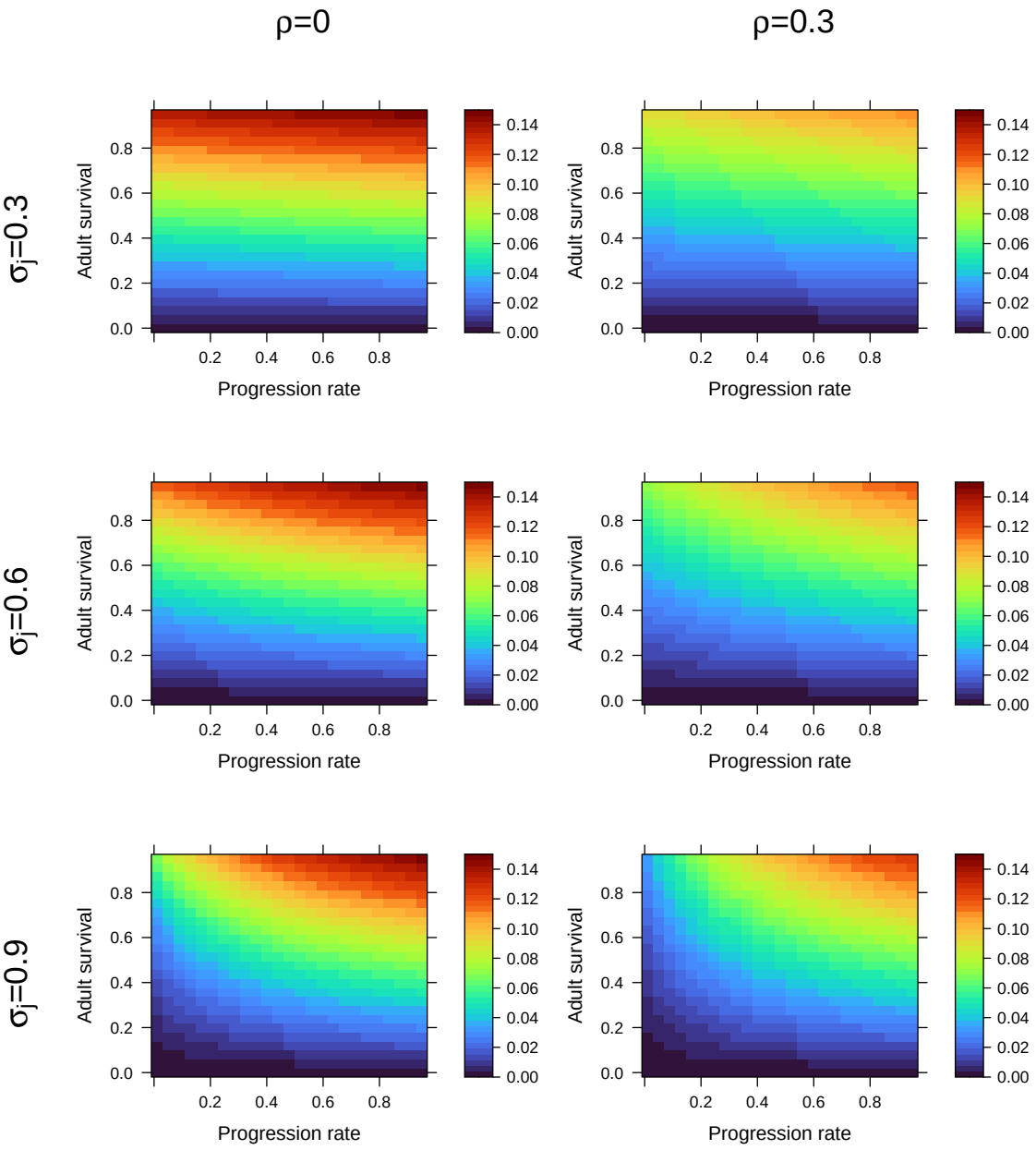

Figure S14: Strength of density effects on resistance when adult survival is density-dependent. Details are the same as Figure S6.

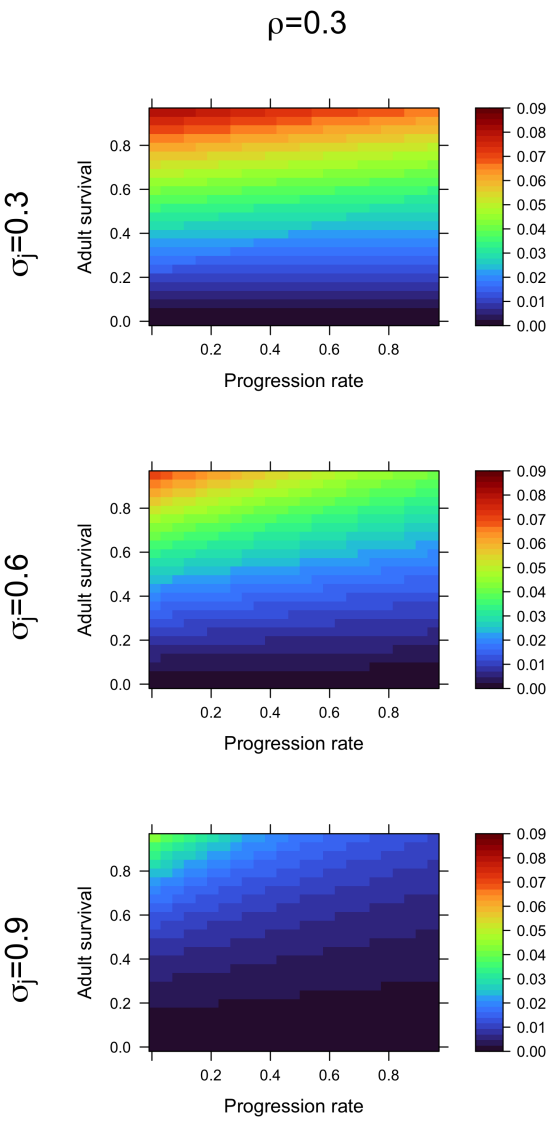

Figure S15: Strength of density effects on resistance when retrogression rate is density-dependent. Details are the same as Figure S6.

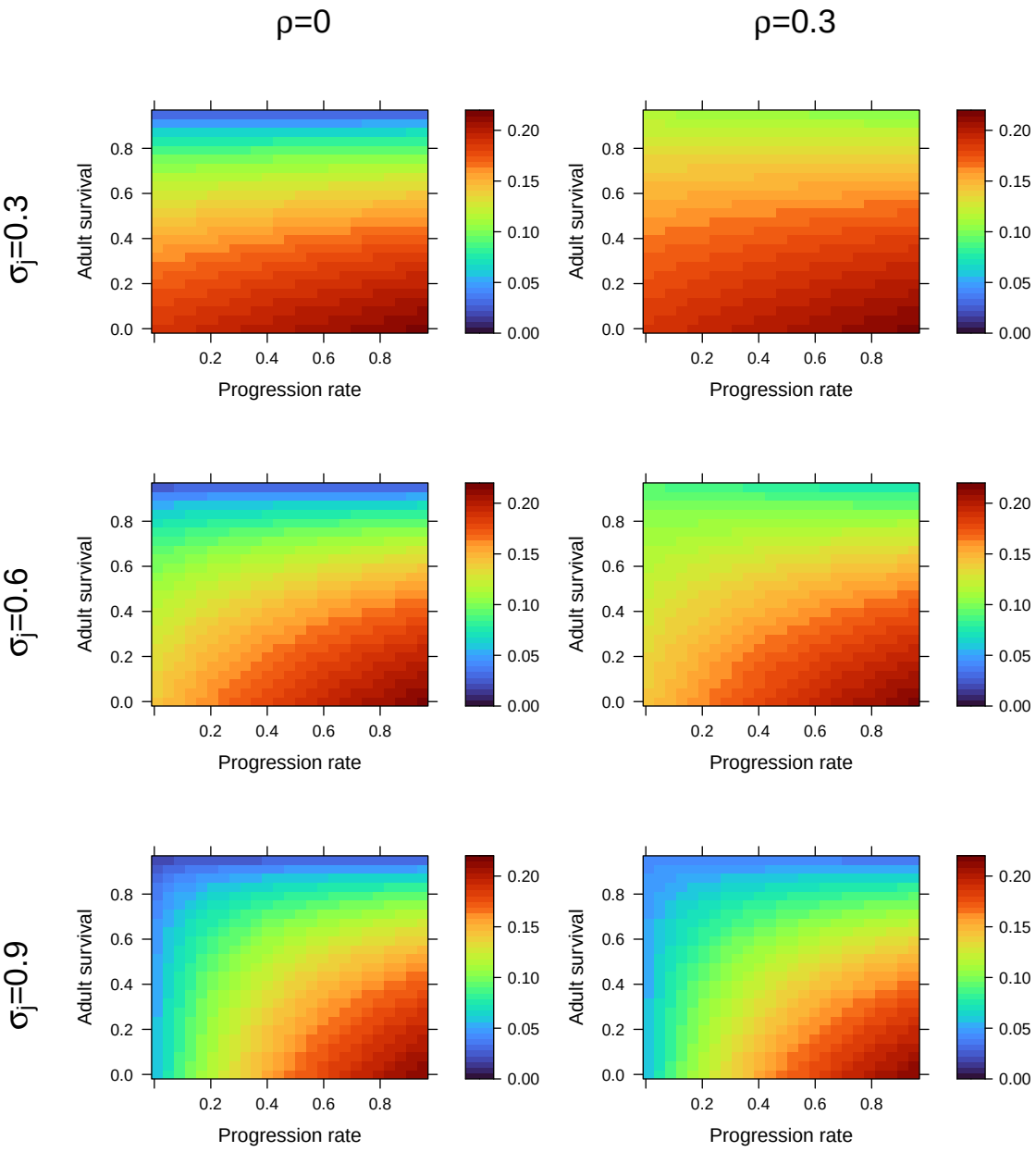

Figure S16: Strength of density effects on resistance when reproductive output is density-dependent. Details are the same as Figure S6.

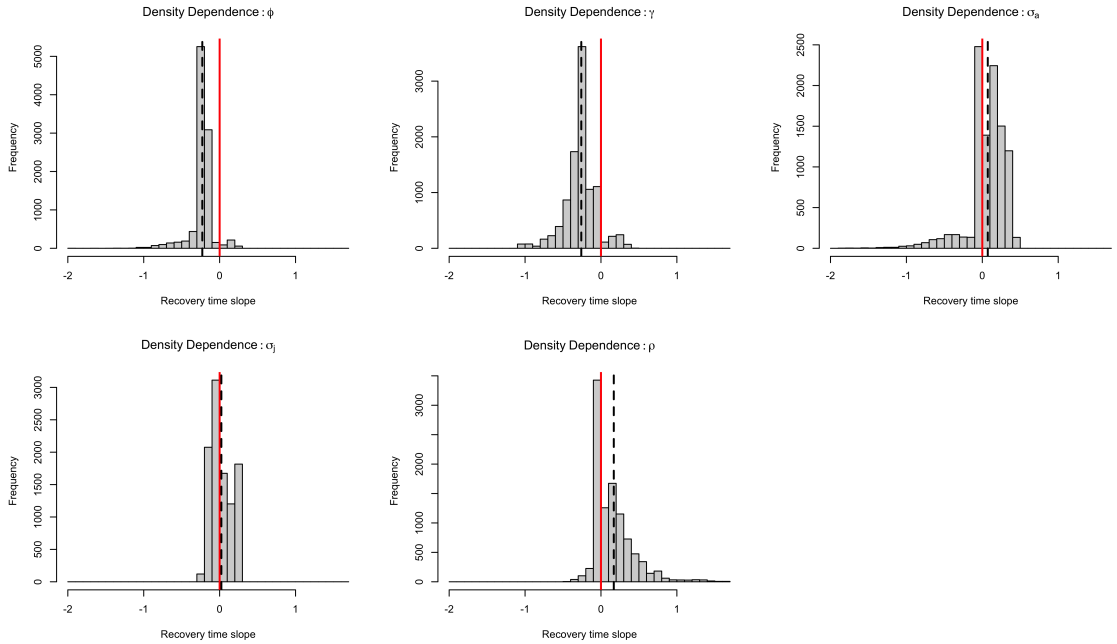

Figure S17: The distribution of recovery time slope values depends on which vital rate is the target of density dependence. Details are the same as in Figure S5.

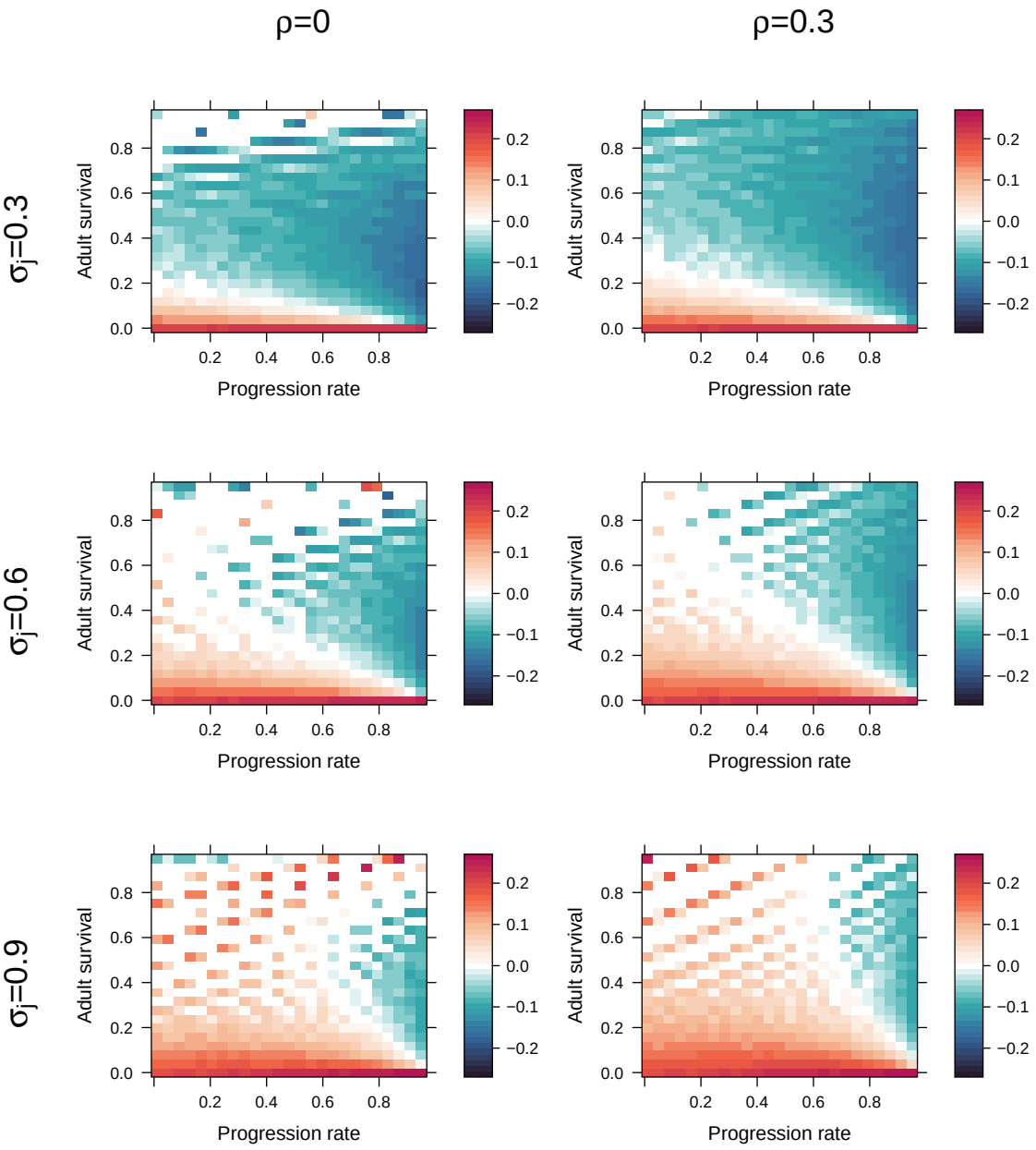

Figure S18: Strength of density effects on recovery time when juvenile survival is density-dependent. Details are the same as Figure S6.

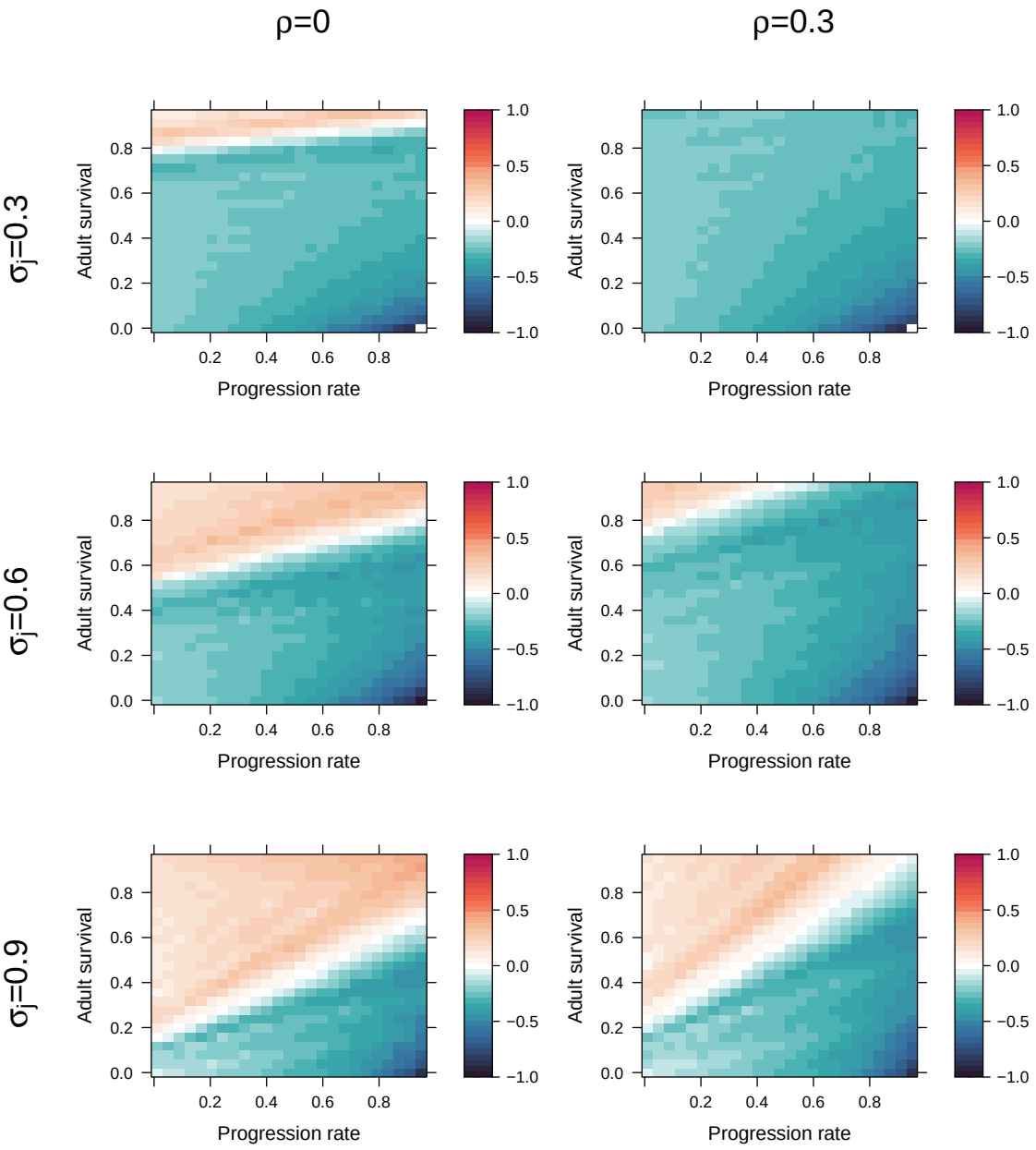

Figure S19: Strength of density effects on recovery time when juvenile progression rate is density-dependent. Details are the same as Figure S6.

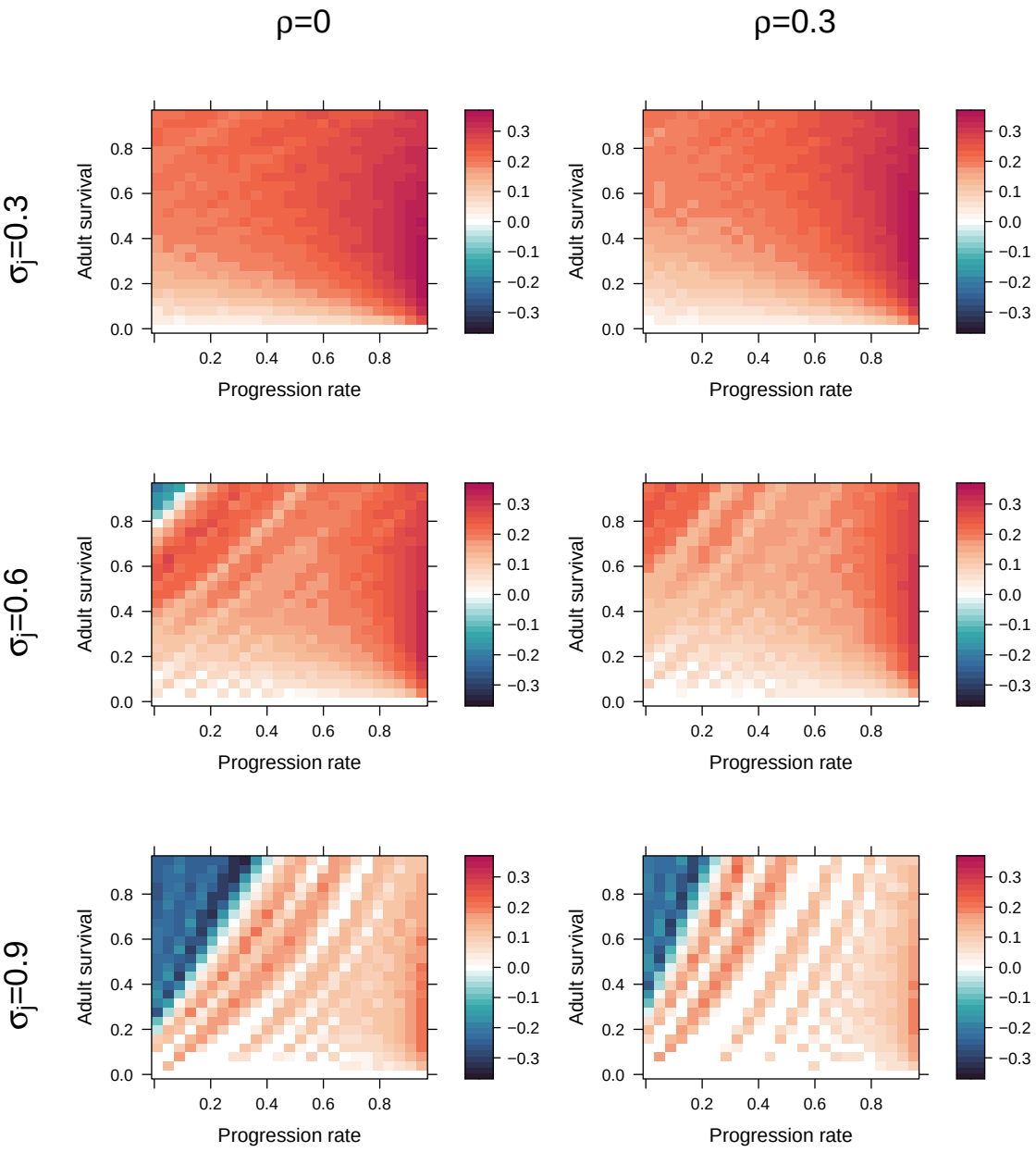

Figure S20: Strength of density effects on recovery time when adult survival is density-dependent. Details are the same as Figure S6.

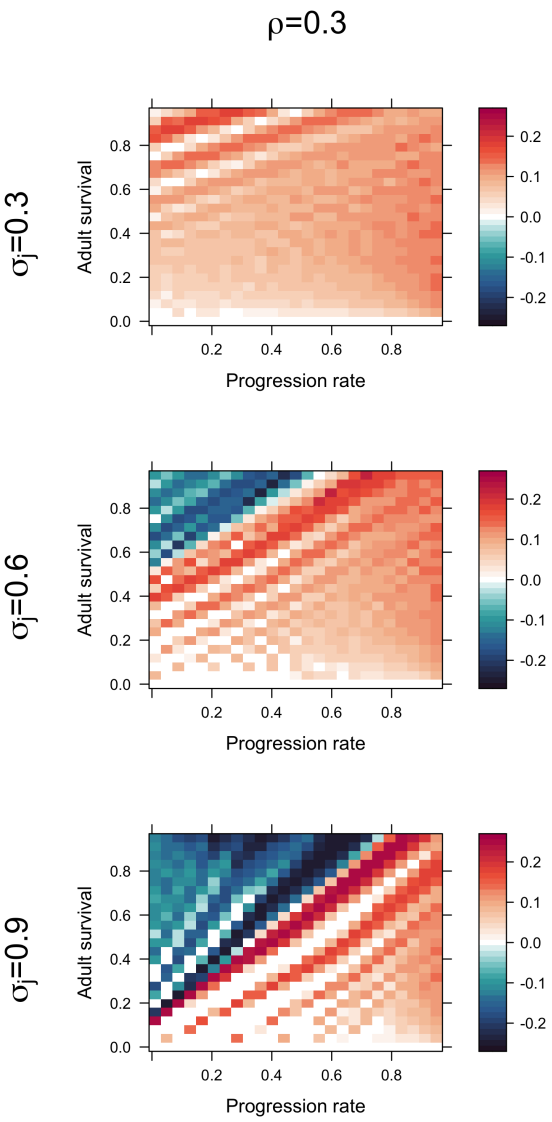

Figure S21: Strength of density effects on recovery time when retrogression rate is density-dependent. Details are the same as Figure S6.

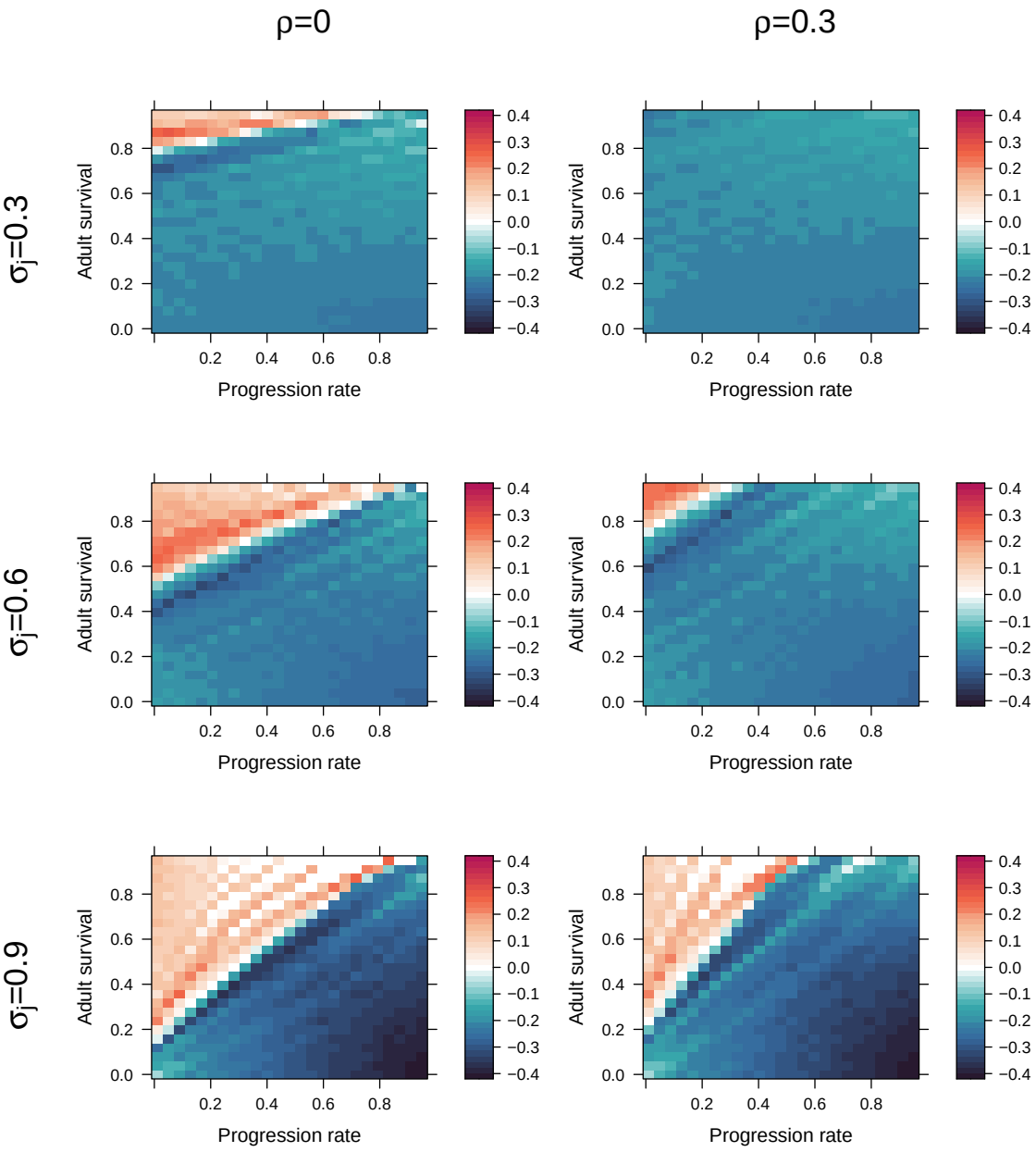

Figure S22: Strength of density effects on recovery time when reproductive output is density-dependent. Details are the same as Figure S6.

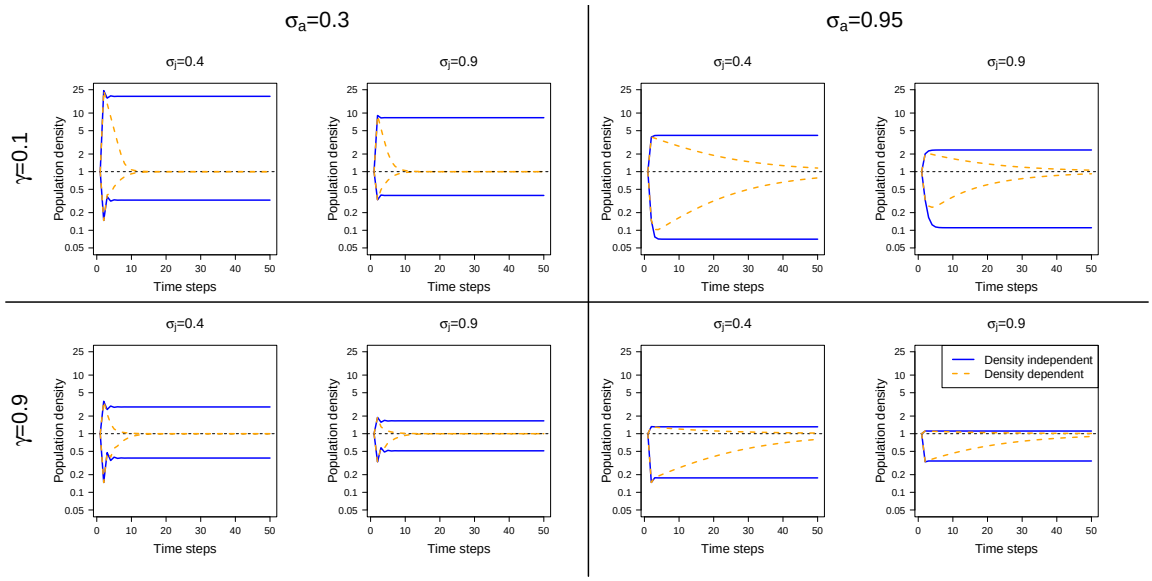

Figure S23: Variation in transient envelope patterns across our set of virtual species and between density-dependent and density-independent models. In this case, density dependence operates on juvenile survival (σ_j).

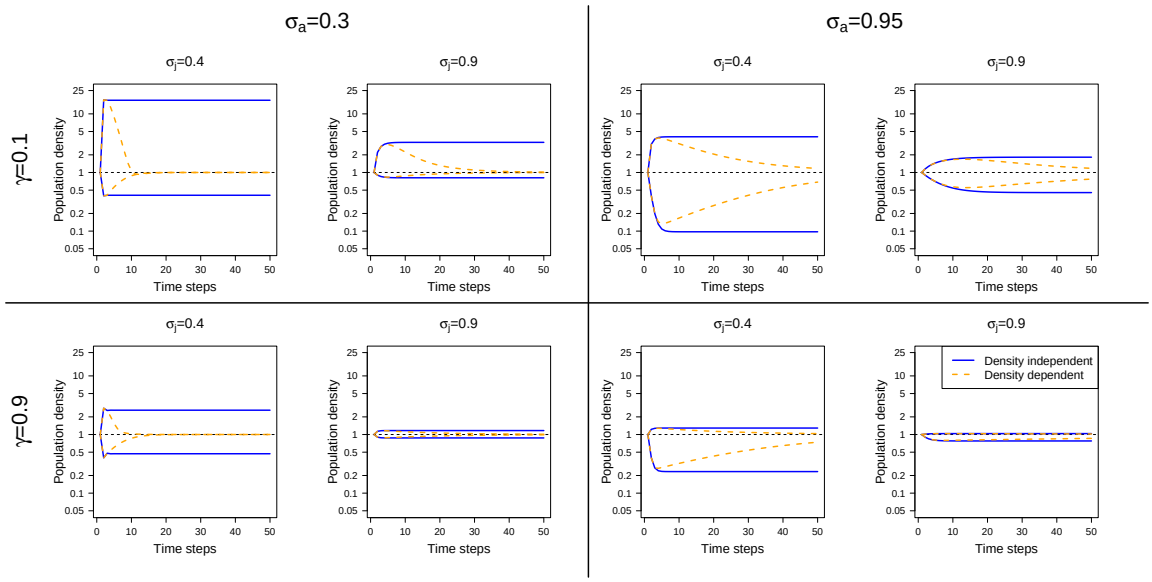

Figure S24: Variation in transient envelope patterns across our set of virtual species and between density-dependent and density-independent models. In this case, density dependence operates on progression rate (γ).

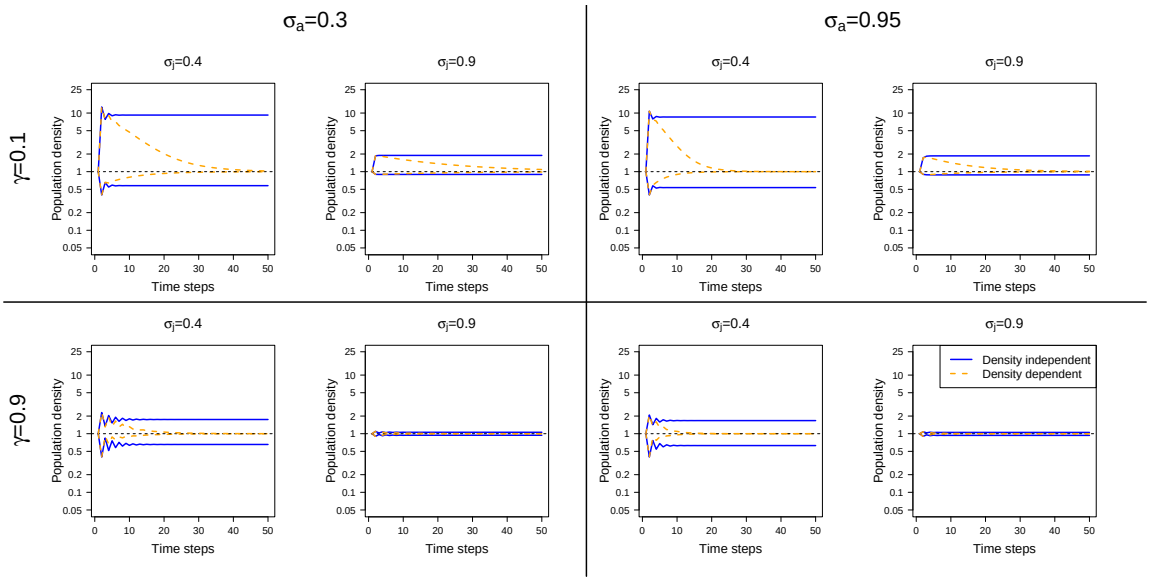

Figure S25: Variation in transient envelope patterns across our set of virtual species and between density-dependent and density-independent models. In this case, density dependence operates on adult survival (σ_a).

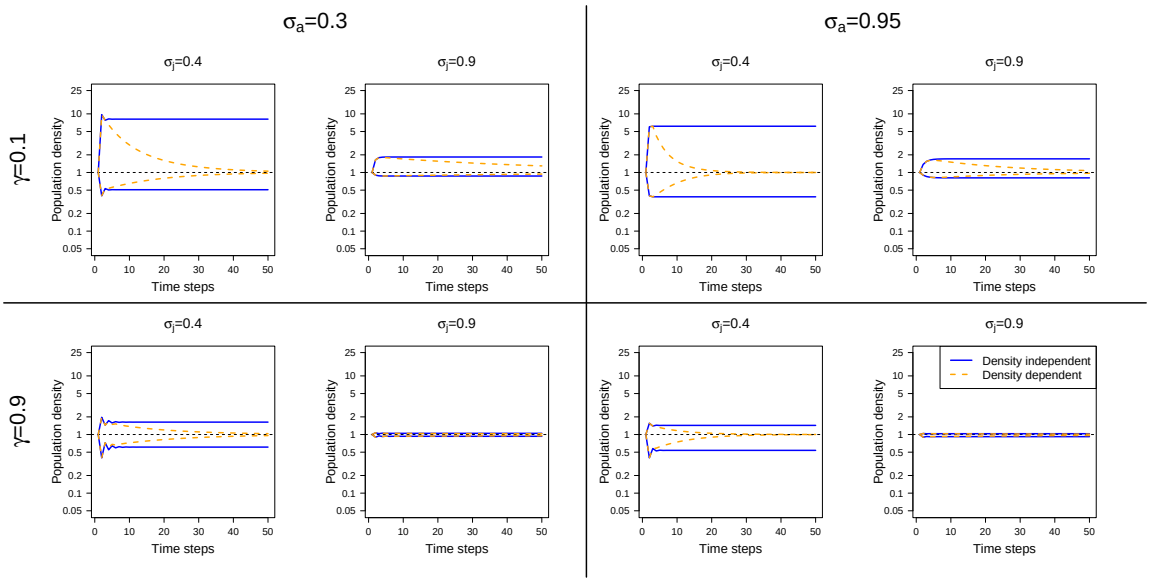

Figure S26: Variation in transient envelope patterns across our set of virtual species and between density-dependent and density-independent models. In this case, density dependence operates on retrogression rate (ρ).

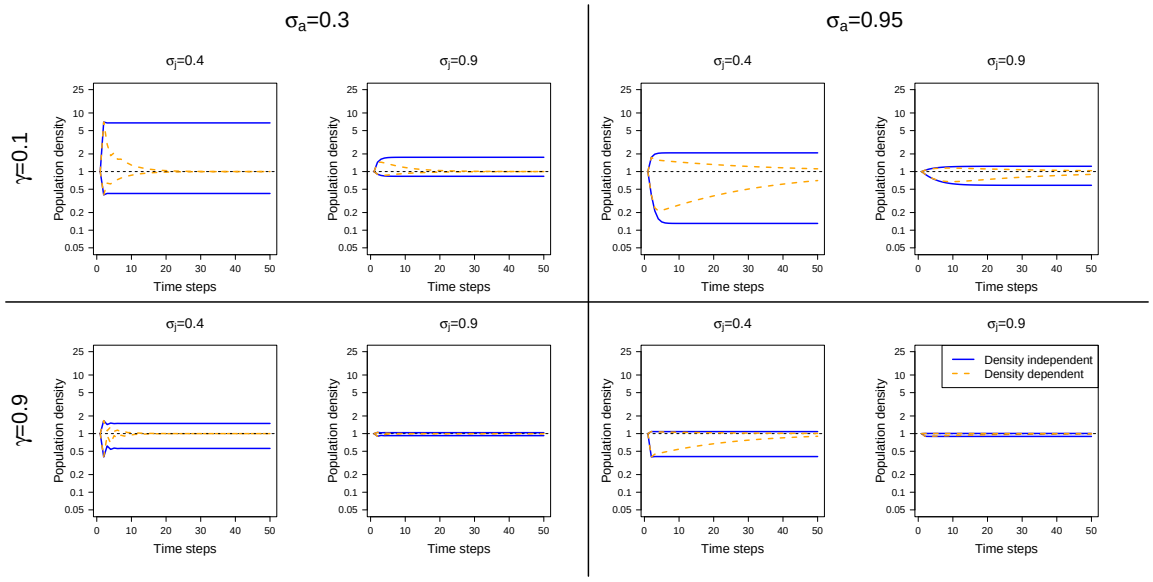

Figure S27: Variation in transient envelope patterns across our set of virtual species and between density-dependent and density-independent models. In this case, density dependence operates on reproductive output (ϕ).

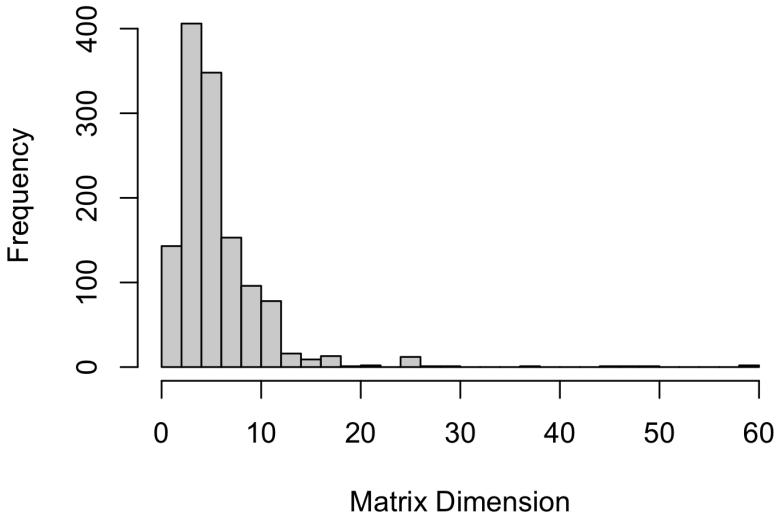

Figure S28: The matrix dimensions for empirical models used in selecting virtual species models. The matrix dimension is the number of classes included in the projection matrix. Before collapsing all the models to 2×2, most of the models were larger, representing more complex life cycles than represented by our two-stage model (Supplemental Materials Table S4).